NASA-TM-2020-5005042

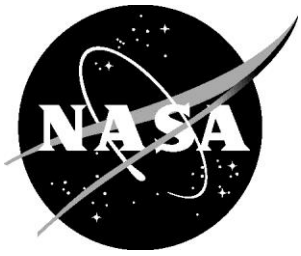

Process for Detecting Strong Convection Using an Airborne, Doppler, Weather Radar

Steven D. Harrah
Langley Research Center, Hampton, Virginia

Patricia J. Hunt
Analytical Mechanics Associates, Inc., Hampton, Virginia

Justin K. Strickland
Analytical Mechanics Associates, Inc., Hampton, Virginia

August 2020

NASA STI Program . . . in Profile

Since its founding, NASA has been dedicated to the advancement of aeronautics and space science. The NASA scientific and technical information (STI) program plays a key part in helping NASA maintain this important role.

The NASA STI program operates under the auspices of the Agency Chief Information Officer. It collects, organizes, provides for archiving, and disseminates NASA's STI. The NASA STI program provides access to the NTRS Registered and its public interface, the NASA Technical Reports Server, thus providing one of the largest collections of aeronautical and space science STI in the world. Results are published in both non-NASA channels and by NASA in the NASA STI Report Series, which includes the following report types:

- TECHNICAL PUBLICATION. Reports of completed research or a major significant phase of research that present the results of NASA Programs and include extensive data or theoretical analysis. Includes compilations of significant scientific and technical data and information deemed to be of continuing reference value. NASA counter-part of peer-reviewed formal professional papers but has less stringent limitations on manuscript length and extent of graphic presentations.

- TECHNICAL MEMORANDUM. Scientific and technical findings that are preliminary or of specialized interest, e.g., quick release reports, working papers, and bibliographies that contain minimal annotation. Does not contain extensive analysis.

- CONTRACTOR REPORT. Scientific and technical findings by NASA-sponsored contractors and grantees.

- CONFERENCE PUBLICATION. Collected papers from scientific and technical conferences, symposia, seminars, or other meetings sponsored or co-sponsored by NASA.

- SPECIAL PUBLICATION. Scientific, technical, or historical information from NASA programs, projects, and missions, often concerned with subjects having substantial public interest.

- TECHNICAL TRANSLATION. English-language translations of foreign scientific and technical material pertinent to NASA's mission.

Specialized services also include organizing and publishing research results, distributing specialized research announcements and feeds, providing information desk and personal search support, and enabling data exchange services.

For more information about the NASA STI program, see the following:

- Access the NASA STI program home page at http://www.sti.nasa.gov

- E-mail your question to help@sti.nasa.gov

- Phone the NASA STI Information Desk at 757-864-9658

- Write to:
  NASA STI Information Desk
  Mail Stop 148
  NASA Langley Research Center
  Hampton, VA 23681-2199

NASA-TM-2020-5005042

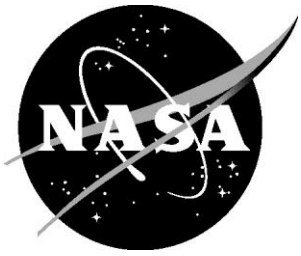

Process for Detecting Strong Convection Using an Airborne, Doppler, Weather Radar

Steven D. Harrah
Langley Research Center, Hampton, Virginia

Patricia J. Hunt
Analytical Mechanics Associates, Inc., Hampton, Virginia

Justin K. Strickland
Analytical Mechanics Associates, Inc., Hampton, Virginia

National Aeronautics and
Space Administration

Langley Research Center
Hampton, Virginia 23681-2199

August 2020

Available from:

NASA STI Program / Mail Stop 148
NASA Langley Research Center
Hampton, VA 23681-2199
Fax: 757-864-6500

Process for Detecting Strong Convection Using an Airborne, Doppler, Weather Radar

Steven D. Harrah
NASA Langley Research Center, Hampton Virginia 23681

Patricia J. Hunt
Analytical Mechanics Associates, Inc., Hampton, Virginia

Justin K. Strickland
Analytical Mechanics Associates, Inc., Hampton, Virginia

ABSTRACT

This document presents a methodology for producing a measure of the convective wind field ahead of an aircraft using a modern, airborne, Doppler, weather radar. The processes and hardware requirements are consistent with the capabilities found in modern commercial weather radars commonly in use on commercial transport aircraft. The fundamental process is developed as well as results from ground and flight testing are described. This application appears sufficiently mature to allow its use in future NASA flight campaigns that will search for convective cells. If this application continues to perform successfully, it will be recommended to avionics manufacturing colleagues for inclusion into future commercial, airborne, Doppler, weather radars to aide pilots with flight operations and further enhance aviation safety.

1 Background

Airborne, Doppler, weather radars have been utilized by the commercial aviation industry for more than three decades; if one includes/considers non-coherent (non-Doppler) radar systems then this record extends several decades further. This technology plays the preeminent role in maintaining safe flights in and around weather systems and the various hazards associated with severe weather. Utilizing this technology, over the past three decades NASA researchers have developed numerous aviation safety applications such as Wind Shear detection, Enhanced Turbulence detection, Air-to-Air Multi-aircraft Tracking, Terrain Awareness, Runway Incursion detection, and Low Visibility Surface Operations capabilities. All of these applications are either: already employed in commercial weather radar systems being flown on every commercial transport aircraft, or they are seeking certification approval prior to deployment into these same commercial weather radar systems. This document summarizes another airborne Doppler weather radar application that has been developed and tested by NASA researchers to improve aviation safety by providing pilots a forewarning of convective activity in their vicinity.

Maintaining or improving aviation safety is one of the directives of NASA's Aeronautics Mission Directorate and advancing the capabilities of commercial avionics systems enables this result. Most of the weather radar advancements, NASA has developed over the past three decades, have focused on changes to the signal and data processing performed in these radars and did not require changes to the basic hardware nor the system's design. This research, development, and design philosophy was intentionally employed to increase the commercialization potential of the results and minimize the deployment cost for these technological enhancements. To many, NASA's aviation safety research, development, and design

processes appear unconstrained by the realities imposed on commercial avionics manufacturers since NASA does not produce a commercial product so designs/concepts do not have to endure the forces that drive the commercial aviation industry. But as a practical matter, NASA's success in improving aviation safety is directly proportional to how well/often results are transferred into commercial products. Consequently, NASA's concepts and design modifications are also constrained by most of the same commercial factors that affect the avionics manufacturing industry. While revolutionary concepts and designs are considered in NASA's technology development processes, often less radical approaches are selected for development since they will provide significant benefit without the cost and delays built into more revolutionary schemes. The challenge for research, development, and design engineers working in this industry is to produce as much benefit as possible from existing technologies with minimal changes to these technologies.

Airborne weather radars can provide pilots with a plethora of information. Basic reflectivity, the false-colored returns often seen on televised weather, portrays how much water is present in a cloud. Modern coherent radars are capable of measuring the subtle Doppler shift produced by the motion of the falling rain thereby sensing wind speeds and direction. By observing this Doppler spectrum and maintaining its geo-reference, other aviation hazards may also be observed. If the winds change speed and direction over a small space then shear is observed and can be assessed as a hazard to aviation. In a similar manner, if there is significant variation in the winds at a single location then turbulence can be observed and assessed as another aviation hazard. In addition to long-range severe weather, wind shear, and enhanced turbulence detection, NASA has developed and flight demonstrated radar-based enhanced vision capabilities such as airborne traffic surveillance, terrain awareness, runway confirmation, and runway object detection applications – all developed from the existing, X-band, weather radars that fly on every commercial transport aircraft. These radar applications have been transferred to the avionics manufacturers and are now the basis for most/all of the radar-based aviation safety products on a modern flight deck.

Many of the weather hazards investigated are produced by convection – rising air currents present in severe storm cells. These regions can be small and localized or they can be large and embedded in even larger weather systems. The strength of these convective regions produces affects that are detrimental to aircraft and dangerous for pilots to operate. So detection and localization of these convective winds would be a great aid to commercial pilots and flight operations. But one limitation imposed by physics on Doppler measurements is that only radial motion can be directly measured; motions in the two orthogonal directions (one of which is vertical) do not contribute to the Doppler process. This paper discusses a method for extracting these vertical wind estimates that does not require any radar hardware changes nor any additional measurements nor any changes to the basic data organization/memory management; instead, it merely requires a few additional computations to be performed.

2 CONVEX Algorithm

The CONVEX algorithm uses two radar sweeps at different tilt angles to compute differences in the two radar radial velocity measurements (for each range bin) to estimate the vertical velocity component of the wind (i.e. convection). The first sweep is set to a tilt angle of zero degrees. Using zero degrees has the benefit of being perpendicular to the vertical velocity and therefore provides an independent measurement of horizontal velocity without a vertical component. The second sweep tilts the antenna downward (negative elevation angle). The tilt angle of the second sweep should be large enough that the two measurements are independent of each other (i.e. non-overlapping beams). There are however restrictions on how large the tilt angle can be due to hardware limitations. The second tilt is also constrained on how far apart vertically the measurements can be taken yet still measure the same portion or region of the weather. In the following description the first sweep tilt angle is set to 0 degrees and the second sweep tilt angle is set to -15 degrees. Each calculation made is for each range bin for a specific area of sky between the two sweeps which includes the horizontal plane from the aircraft.

Let the Wind Vector be defined by:

$$\vec{V} = V_\rho \hat{\rho} + V_\varphi \hat{\varphi} + V_V \hat{z}$$

and the radar look vector defined as:

$$\vec{R}(\theta) = \cos\theta \hat{\rho} + \sin\theta \hat{z}$$

where $\hat{\rho}$ is the radial unit vector and $\hat{z}$ is the vertical unit vector, and θ is the tilt (elevation) angle[1] in a cylindrical coordinate system as shown graphically in the figure on right.

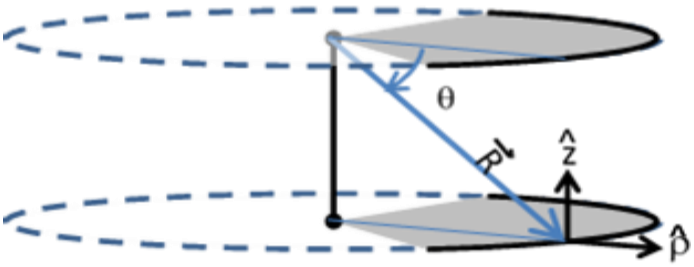

Cylindrical coordinate system used to define wind vector and radar look vector. Range bin located at (R,θ) and at azimuth angle ϕ.

The measured radial wind is the dot product of these two vectors: [2]

$$V_R(\theta) = \vec{V} \bullet \vec{R} = V_\rho \cos\theta + V_V \sin\theta$$

So for θ = 0° (horizontal plane),

$$\vec{R}(0°) = 1\hat{\rho} + 0\hat{z} \quad \text{and} \quad \vec{V} \bullet \vec{R} = V_\rho$$

similarly, for θ = -15°,

$$\vec{V} \bullet \vec{R} = V_\rho \cos(-15°) + V_V \sin(-15°)$$

Since the winds are assumed consistent (i.e. uniform over this short vertical extent) then the last equation above can be solved for V_v using the θ=0° value for V_ρ and the measurement at θ=-15° for the value of the dot product (LHS). This results in,

$$V_V = \frac{[V_R(-15°) - (V_R(0°) * \cos(-15°))]}{\sin(-15°)}$$

Tests of this expression have validated this result; naturally, performance will be limited by small-scale, non-uniformity of the wind field and the ability to vertically associate measurements at the two different elevations while accounting for aircraft motion.

2.1 Compensating for Platform Translation

While the ability to accurately associate range bins so that they are vertically stacked is a key attribute in defining the performance of the vertical wind estimate, even if this association is performed perfectly the fact that the platform has moved during the time period between measurements creates a different dot product between the horizontal component of wind and the look vector. This difference creates a different estimate for the horizontal component which then translates into an ever increasing bias on the vertical estimate. This bias will produce an artifact in the vertical velocity display which is not actually present in

[1] As shown in the figure, θ will have a negative value.
[2] The φ component of the wind field is always perpendicular to the look vector and thus contributes nothing to radar wind measurments.

the wind field. The process below corrects/compensates for the aircraft motion (translation) and thereby restores the performance of the vertical wind estimate.

The two sweep process described above (denoted the "two-bar sequence") can be improved by adding a third sweep (referred to as the "three-bar sequence"). By using multiple sweeps, multiple look angles are produced for each resolution cell thereby allowing an estimate of the full wind vector to be produced. In other words, the three-bar sequence resolves the horizontal velocity direction and magnitude components thereby improving the vertical velocity estimate, whereas the two-bar sequence does not. If these sweeps use alternating horizontal and tilted scans, then the velocity measurements they produce of a common spatial location (see figure below) are given by:

$$V_i = V_H cos\,\alpha_i \qquad \text{current horizontal scan}$$

$$V_{-1} = V_H cos\,\alpha_{-1} cos\,\theta + V_V sin\theta \qquad \text{previous tilted scan}$$

$$V_{-2} = V_H cos\,\alpha_{-2} \qquad \text{oldest horizontal scan}$$

where V_i is the measured velocity (resulting from the dot product of the wind and look vectors at platform position *i*), V_H is the horizontal wind magnitude, α_i is the angle between the horizontal wind vector and the horizontal look vector at platform position *i*, and θ_i is the tilt (elevation) angle of the look vector at platform position *i* (as seen in the graphic to the right, three platform positions denoted (P_i,P_{-1},P_{-2}) –this index refers to a sweep count used in this process). Three distinct look angles are required to resolve the three components of the wind vector.

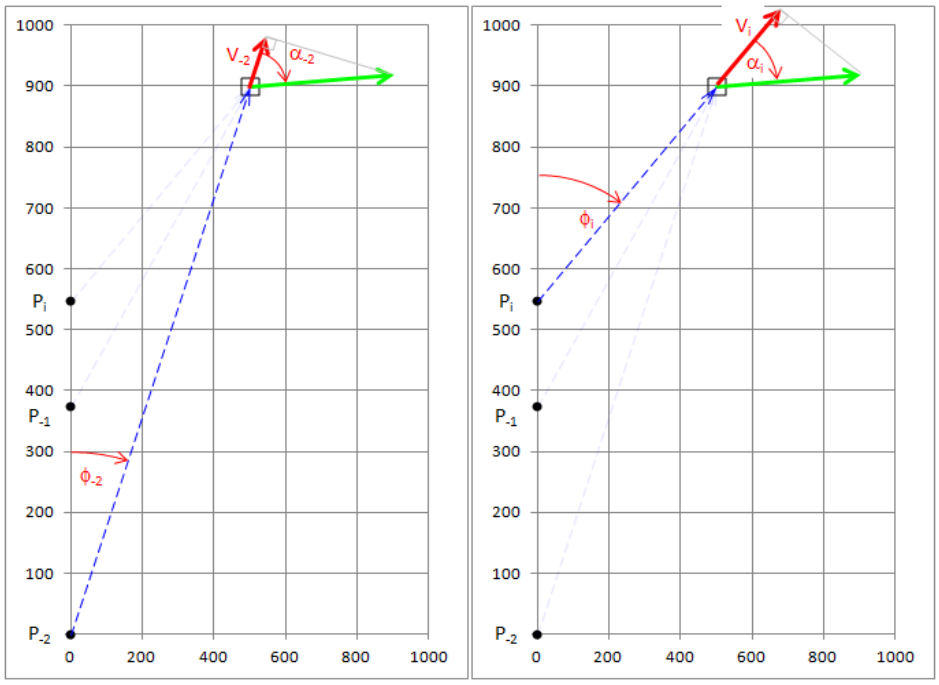

For straight translation of the platform, the angles are related through

$$\alpha_T = \varphi_i + \alpha_i$$

where α_T is the total angle between the longitudinal axis of the platform and the wind vector, φ_i is the azimuth angle, and α_i is the angle described above. The ratio of the horizontal measurements produces:

$$\frac{V_{-2}}{V_i} = \left[\frac{V_H \cos\alpha_{-2}}{V_H \cos\alpha_i}\right] = \left[\frac{\cos(\alpha_T - \varphi_{-2})}{\cos(\alpha_T - \varphi_i)}\right]$$

Using the trigonometric identities:

$$\cos(A \pm B) = \cos(A)\cos(B) \mp \sin(A)\sin(B) \quad \text{and} \quad \tan(C) = \frac{\sin(C)}{\cos(C)}$$

the ratio expression above reduces to

$$tan(\alpha_T) = \left[\frac{V_i cos\varphi_{-2} - V_{-2} cos\varphi_i}{V_{-2} sin\varphi_i - V_i sin\varphi_{-2}}\right]$$

which can be solved for α_T (the angle between the longitudinal axis of the platform and the horizontal wind vector). Using α_T and either equation for V_i or V_{-2}, V_H may be computed from

$$V_H = \frac{V_i}{cos\ \alpha_i} = \frac{V_i}{\cos(\alpha_T - \varphi_i)}$$

The most sensible process would use the latest value (i.e., V_i) since it should be from a shorter range and therefore a higher SNR than the older value V_{-2}. But if the measurement is looking perpendicular to the wind vector then this expression will fail as the denominator approaches zero near $\alpha_i = 90^o$. However, under this scenario the apparent (i.e. measured) horizontal velocity should be equal to zero and may be assigned rather than calculated: if $\alpha_i \approx 90^o$ then $V_H = 0$, else compute V_H using the expression above.

Using the values for α_T and V_H, the vertical velocity can be estimated using the original V_V expression to produce

$$V_V = \frac{V_{-1}(\theta) - |V_H| \cos(\alpha_T - \varphi_{-1}) \cos\theta}{\sin(\theta)}$$

where V_V is the vertical velocity, V_{-1} is the radial velocity measured at platform position *-1* and assumed to be at a non-zero elevation angle θ.

2.2 Alternate Scan Sequence

The previous section described the use of three scans to calculate the wind vector (V_H, α_T, V_V); however, these scans use the elevation sequenced 0^o, θ^o, and 0^o where θ is a non-horizontal (tilted) scan (e.g. expressed as -15^o in the section 2 of this document). In a typical radar the next scan (the fourth in this sequence) would likely be at the non-horizontal elevation which can be used to produce an alternate three scan sequence: θ^o, 0^o, and θ^o. This three scan sequence will be referred to as the alternate three-bar sequence. Using the nomenclature from the previous section, the equations that describe the measured wind velocity for these three scans are:

$V_i = V_H \cos(\alpha_T - \varphi_i)\cos\theta + V_V \sin\theta$ current scan & second tilted scan

$V_{-1} = V_H \cos(\alpha_T - \varphi_{-1})$ second scan & only horizontal scan

$V_{-2} = V_H \cos(\alpha_T - \varphi_{-2})\cos\theta + V_V \sin\theta$ oldest scan of three & first tilted scan

While these three scans have sufficient information to calculate the wind vector, the equations used to calculate the wind vector components for this sequence differ slightly from those used for the other 3-scan sequence and from those used for the two-horizontal scan sequence developed in the previous sections. The

wind vector for a two-elevated, one-horizontal scan sequence (with the horizontal scan between the two elevated scans) is given by,

$$\alpha_T = -\tan^{-1}\left[\frac{\cos\varphi_{-1}\left(\frac{V_i - V_{-2}}{V_{-1}\cos\theta}\right) - (\cos\varphi_i - \cos\varphi_{-2})}{\sin\varphi_{-1}\left(\frac{V_i - V_{-2}}{V_{-1}\cos\theta}\right) - (\sin\varphi_i - \sin\varphi_{-2})}\right]$$

$$V_H = \frac{V_{-1}}{\cos(\alpha_T - \varphi_{-1})}$$

$$V_V = \frac{V_i - |V_H|\cos(\alpha_T - \varphi_i)\cos\theta}{\sin\theta}$$

2.3 Compensating for Platform Rotation

In addition to platform translation, the platform can/will rotate. Changes in roll and pitch are compensated for by the radar hardware (i.e. pedestal), but yaw and/or heading change are not; so it is necessary to consider what rotational compensation is required to allow the vertical velocity calculation to be performed. It's important to remember that the radar (0^o,0^o) angular reference is the longitudinal axis of the aircraft and since the radar doesn't compensate for yaw (instantaneous angular difference between track and heading), the association process must account for heading changes. At any point in space or time, the radar measurements used for this development are relative to the radar's frame of reference, and the equations developed above do not need <u>any</u> adjustment for the current (i^{th}) sweep. However, in order to associate the current bin with a previous bin, both translation and rotation must be accounted for (in the current development this is accomplished by translating and rotating the view point from CPI frame-to-CPI frame; thus the array address for the associated cell is the same as the current cell only in the old "bit plane").

If the radar azimuth and aircraft heading (Θ_i) are stored for each array cell then they can be used to compensate for rotational changes that occurred since the data was measured (i.e., these "old" values are part of the -2 sweep and must have this compensation to allow them to be used in the α_T and V_V calculations). As may be seen in the adjoining figure, a heading change does not affect the magnitude of the dot product; instead, the rotation only redefines the azimuth angle – neither the blue look-vector nor the red V_{-2} vector (result of dot product between look-vector and "green" wind vector) change due to a change in heading ($\Delta\Theta$) only the apparent azimuth angle is increased or decreased by the change in heading. Note a positive heading change (clockwise in figure) decreases the apparent azimuth angle thus

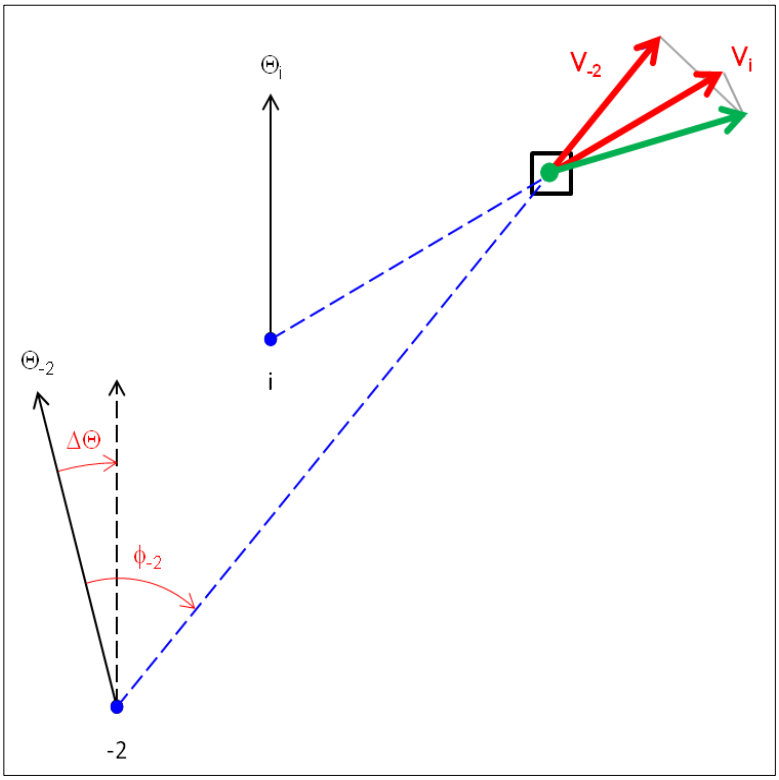

$$\phi'_{-2} = \phi_{-2} - \Delta\Theta_{-2}$$

where $\Delta\Theta_{-2} = \Theta_{-2} - \Theta_I$ The equations for α_T and V_V remain the same only substituting ϕ' for ϕ.

3 Ground Test Assessment

A modern commercial Doppler, weather radar was used to assess the CONVEX concept. This radar was installed onto the mobile radar lab at NASA Langley Research Center and operated on rainy days, when there were sufficient returns to obtain reflectivity and therefore velocity measurements for a wide range of altitudes from the minimum range up to the top of the cloud layer. These velocity measurements were then compared to NOAA reported weather conditions to validate the signal processing algorithms.

3.1 Ground Test Description

The rack mounted equipment was mounted inside the van and the antenna with pedestal was installed on top of the van pointing upward. The radar transceiver was set up with a 1 microsecond pulse width, which resulted in a range bin size of 150 meters. The first range bin was located about 900 meters from the antenna. Sixty three range bins of data were collected, producing an overall range of 10km. The antenna had a beam width of 4 degrees in both azimuth and elevation and was scanned ±60 degrees in azimuth. The antenna was oriented so when scanning in azimuth the positive direction was toward the driver's side and the negative azimuth angles were on the passenger side of the van. The antenna tilt angles were oriented so the negative angles were toward the rear of the van and the positive angles were toward the cab or forward part of the van. The CONVEX algorithm computes a component of velocity vector perpendicular to the radar scan plane at zero elevation angles. In this ground test orientation, the algorithm results in horizontal wind speed along an axis running from the rear of the van toward the front. In addition, at an azimuth angle

of zero and an elevation angle of zero, direct Doppler measurements provide velocity along a vertical axis.

The radar data was collected using an alternating tilt sequence from sweep to sweep. The tilt angles used in this sequence are a sweep at a tilt of 0 degrees followed by a sweep at -15 degree tilt and then back to a sweep at a 0 degree tilt. This combination results in sweeps from -60 degrees to +60 degrees in azimuth at a 0 degree tilt and then back from +60 to -60 at a -15 degree tilt. Since the platform during the ground tests is not moving, the two-bar sequence equations are used to make the CONVEX velocity calculations described in Section 2. The three-bar sequence equations described in Section 2.1 and Section 2.2 reduce to the two-bar sequence equations since α_i is constant without platform motion. This results in a vertical profile (up to 10km or ~30,000 ft in altitude) of horizontal winds from the algorithm calculations. Therefore, a direct comparison of the horizontal winds calculated by the convection calculations can be made to the weather conditions reported for each day. See Figure 1 for example of the van setup.

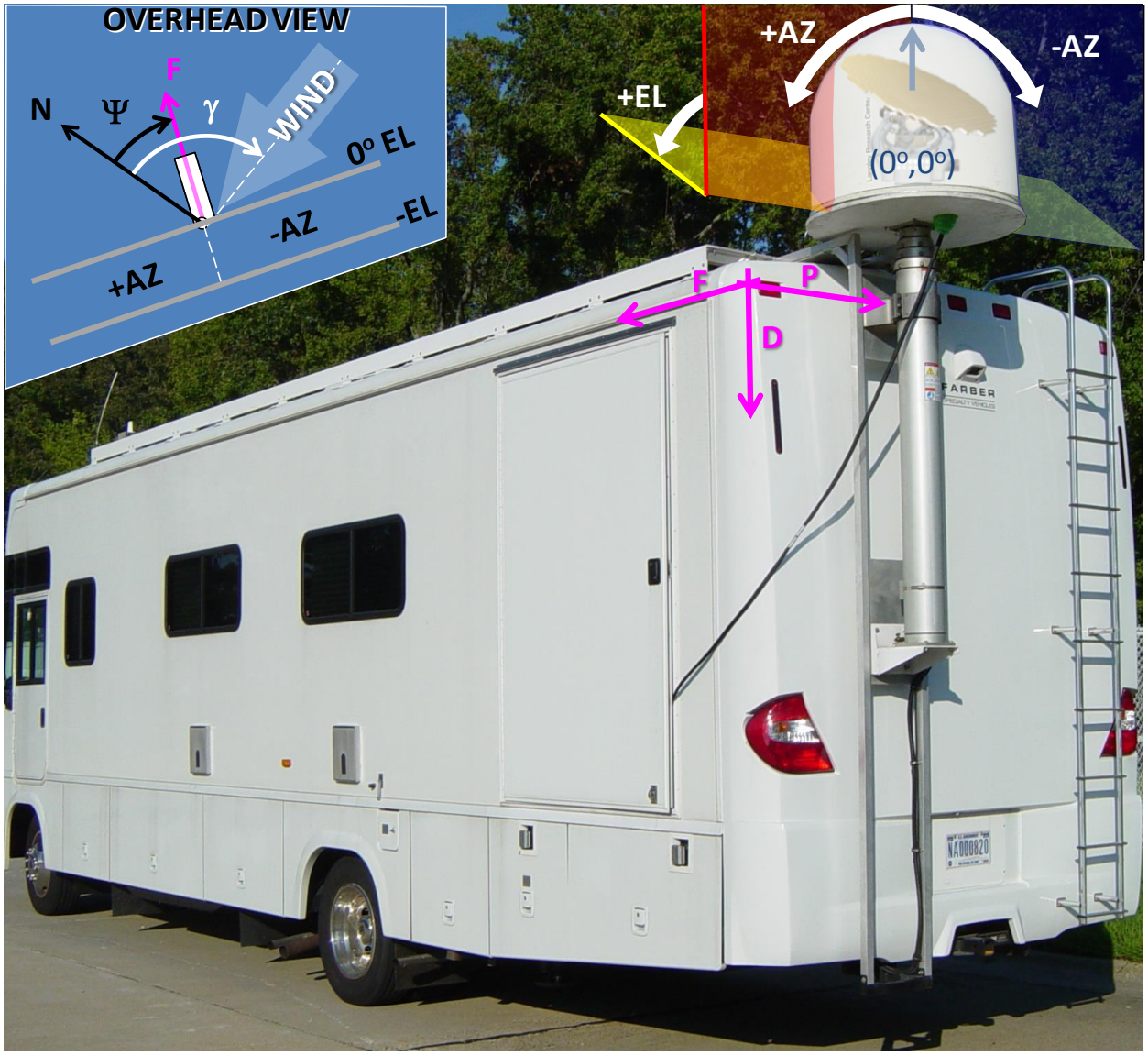

Figure 1: Weather radar configuration on mobile van for ground test

About 240 minutes of radar data was collected from February 7, 2014 through March 6, 2014 using the van with the antenna pointing up into the sky. A summary of all the data collected is in a table in Appendix A. Most of the data was collected with the van parked near the building and facing about 30 degrees toward the east of true north. Day-by-day differences in wind speed and direction provide varying conditions for a fixed orientation. During rain on February 26, 2013, the van was driven in a parking lot and parked in different orientations to obtain different wind directions from the scan direction of the antenna. Multiple sets of data were collected at various orientations. In most cases, a specific orientation relative to the ambient wind direction was selected and held constant during data collection. In one case, the van was driven around in a circle while data was collected at varying orientations.

For comparison, the NOAA reports surface winds and winds aloft data for various altitudes at certain airports. Wind speed and direction are reported at select times of the day. Unfortunately, this information is not readily available for Langley Air Force Base or Newport News Williamsburg International Airport (PHF). Therefore, when available, reported wind conditions from Norfolk International Airport (ORF) and Richmond International Airport (RIC) – for times before and after radar measurements were taken – are used for comparison. Given significant geographic distances, sparse altitude sets, and large time intervals between the reported data points, only a coarse grid of ambient velocities is available for comparison. The data collected for each day can be seen in the table in Appendix A.

3.2 Analysis Approach

There are two approaches for comparing reported wind conditions to radar measurements. The first is to transform reported weather conditions into a radar-centric coordinate system and replicate an expected plan position indicator (PPI) display to perform a qualitative assessment. The second is to transform radar velocity measurements into an Earth-centric coordinate system to conduct a quantitative analysis.

3.2.1 Derivation

By defining an Earth-fixed, North-East-Down (NED) right-hand Cartesian coordinate system, the coordinate transformation from reported wind conditions to the ambient wind field is given by:

$$\begin{bmatrix} \dot{N} \\ \dot{E} \\ \dot{D} \end{bmatrix} = \begin{bmatrix} \cos\gamma & -\sin\gamma & 0 \\ \sin\gamma & \cos\gamma & 0 \\ 0 & 0 & 1 \end{bmatrix} \begin{bmatrix} -V_w \\ 0 \\ V_p \end{bmatrix}$$

Where:

the coordinate transformation matrix is for a positive rotation about the D-axis

$\dot{N}$ is the velocity along the N-axis ($\frac{dN}{dt}$)

$\dot{E}$ is the velocity along the E-axis ($\frac{dE}{dt}$)

$\dot{D}$ is the velocity along the D-axis ($\frac{dD}{dt}$)

γ is the reported direction of the wind (measured from North)

V_w is the reported wind speed

V_p is the downward velocity due to precipitation

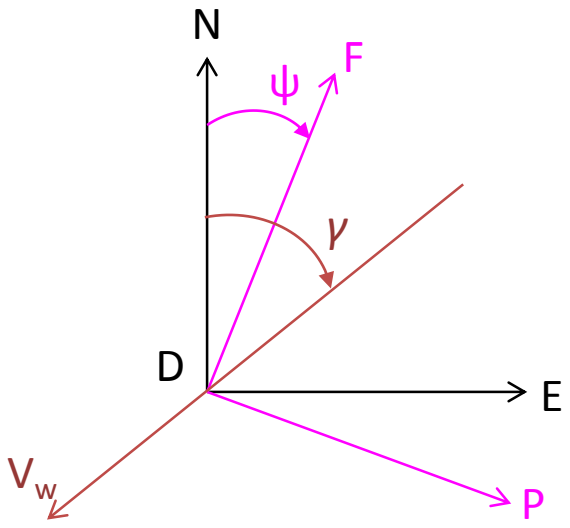

By defining a van-fixed, Front-Passenger-Down (FPD) right-hand Cartesian coordinate system, the

coordinate transformation from the Earth-fixed NED systems is given by:

$$\begin{bmatrix} F \\ P \\ D \end{bmatrix} = \begin{bmatrix} \cos\psi & \sin\psi & 0 \\ -\sin\psi & \cos\psi & 0 \\ 0 & 0 & 1 \end{bmatrix} \begin{bmatrix} N \\ E \\ D \end{bmatrix}$$

or

$$\overrightarrow{FPD} = [\boldsymbol{H}]\overrightarrow{NED}$$

where:

F is the longitudinal axis of the van pointing out the front
P is the lateral axis of the van pointing out the passenger size
D is the vertical axis of the van point downward
[$\boldsymbol{H}$] the coordinate transformation matrix is for a positive rotation about the D-axis
ψ is the heading of the van (measured from North)[3]

By defining a radar-fixed, Range-Scan-Tilt (RST) right hand Cartesian coordinate system, the coordinate transformation from the FPD system is given by:

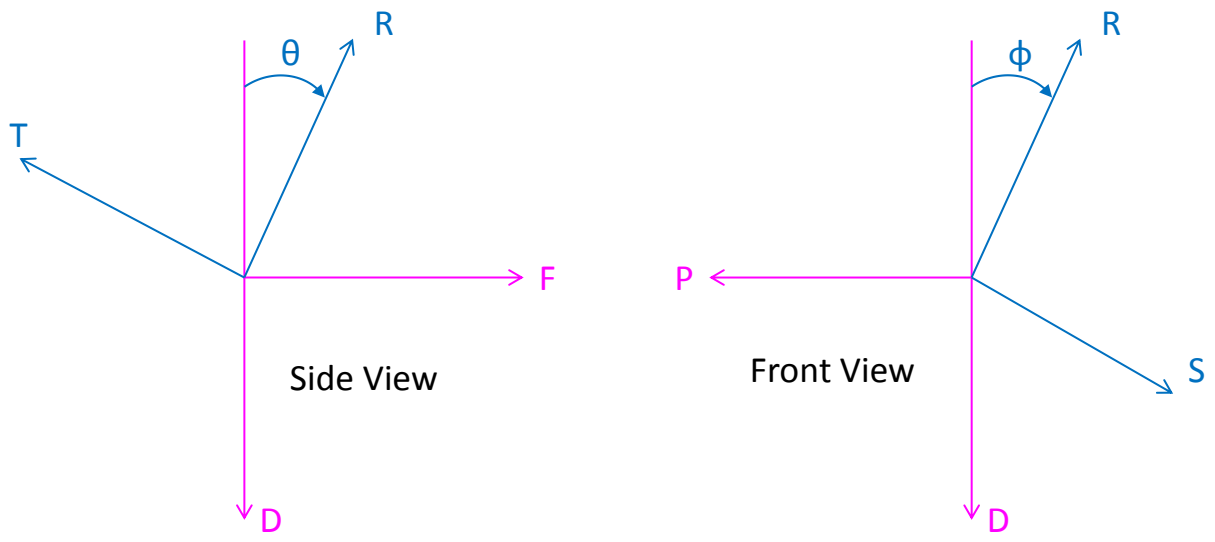

$$\begin{bmatrix} R \\ S \\ T \end{bmatrix} = \begin{bmatrix} \cos\theta & 0 & -\sin\theta \\ 0 & 1 & 0 \\ \sin\theta & 0 & \cos\theta \end{bmatrix} \begin{bmatrix} \cos\varphi & \sin\varphi & 0 \\ -\sin\varphi & \cos\varphi & 0 \\ 0 & 0 & 1 \end{bmatrix} \begin{bmatrix} 0 & 0 & -1 \\ 0 & -1 & 0 \\ -1 & 0 & 0 \end{bmatrix} \begin{bmatrix} F \\ P \\ D \end{bmatrix}$$

or

$$\overrightarrow{RST} = [\boldsymbol{A}][\boldsymbol{B}][\boldsymbol{C}]\overrightarrow{FPD}$$

[3] Van heading denotes vehicle forward facing direction whereas wind direction denotes the prevailing direction the wind comes from. That is, if van heading and wind direction are the same ($\psi = \theta$), the van would experience a direct head wind.

where:

R is an axis aligning with the antenna line-of-sight pointing away from the antenna
S is orthogonal to the R-axis in the scan plane pointing in the direction of positive azimuth
T is orthogonal to the scan plane pointing in the direction of negative elevation
[***A***] is the coordinate transformation matrix for a positive rotation about the S-axis
θ is the antenna elevation (tilt) angle
[***B***] is the coordinate transformation matrix for a positive rotation about the T-axis
φ is the antenna azimuth angle
[***C***] is the coordinate transformation matrix for the radar orientation relative the van

It is important to note that due to the radar mount orientation and the antenna gimbal design, the only correct coordinate rotation order is 1-3-2 (i.e. rotate about the R-axis first, the T-axis second, and the S-axis third). The antennal gimbal does not rotate about the R-axis, however changing the van heading accomplishes an equivalent rotation. The coordinate transformations above are consistent with this rotation order.

3.2.2 Qualitative Assessment

To construct the expected PPI displays, the reported wind speeds and assumed precipitation rates are mapped into the radar line-of-sight to compute expected Doppler measurements. This mapping is given by:

$$\dot{R} = -V_w \sin\theta \cos(\psi - \gamma) - V_w \sin\varphi \cos\theta \sin(\psi - \gamma) - V_p \cos\varphi \cos\theta$$

where:

$\dot{R}$ is the velocity along the R-axis ($\frac{dR}{dt}$) and equivalent to V_R

Likewise, the CONVEX algorithm computes a component of the wind speed aligned with the longitudinal axis of the van. This mapping of the wind speed to compute the expected result is given by:

$$\dot{F} = -V_w \cos(\psi - \gamma)$$

where:

$\dot{F}$ is the velocity along the F-axis ($\frac{dF}{dt}$) and equivalent to V_V

The velocity displays can then be replicated using the reported winds as the radar would observe them. The result is a set of contour plots mimicking the format and color mapping of the displays as best as possible.

3.2.3 Quantitative Analysis

To conduct the quantitative analysis, radar velocity measurements are used to compute ambient wind speed and direction for comparison to the NOAA reported conditions. This approach is more complicated since Doppler measurements can only provide radial velocity along the antenna line-of-site axis (R-axis) while tangential velocities (S-axis and T-axis) remain immeasurable. There are a variety of methods for resolving the tangential velocity components by using multiple measurements at differing scan (azimuth and elevation) angles.

One method is to use the CONVEX algorithm (which computes a horizontal velocity in this case) to

provide a component of the velocity vector in the horizontal plane. Furthermore, if it is assumed that vertical motion, at a given altitude, is steady and uniform over the field-of-regard, velocity measurements along the vertical axis ($\varphi = \theta = 0^0$) can be used to provide a component of the velocity vector in the vertical plane. A three-dimensional velocity vector can then be resolved from the radar measurements and thus wind speed and direction computed.

The coordinate transformation from the FPD system into the RST system yields:

$$\dot{R} = \dot{F}\sin\theta - \dot{P}\sin\varphi\cos\theta - \dot{D}\cos\varphi\cos\theta$$

It is possible to estimate $\dot{D}$ by utilizing the fact that at zero scan angles ($\varphi = \theta = 0^0$) this reduces to: $\dot{R} = \dot{D}$, which is provided by direct velocity measurement ($-V_R$). By taking several velocity measurements at zero scan angles, the mean is found for each altitude. If it is assumed to be constant (at a given altitude) over the entire field-or-regard, then it is possible to solve for all three components of the measured velocity vector in the FPD coordinate frame.

Substituting the measured radial velocity, the CONVEX algorithm result, and the resulting mean D-axis velocity into the above equation and solving for the P-axis term yields:

$$\dot{P} = \frac{-V_R + V_V\sin\theta - \overline{\dot{D}}\cos\varphi\cos\theta}{\sin\varphi\cos\theta}$$

where:

$\overline{\dot{D}}$ is the mean of the velocity measurements taken at zero scan angles

It can be seen that the coordinate transformation results in a singularity at zero azimuth angle ($\varphi = 0^0$) where the radar line-of-site (R) is orthogonal to the P-axis. This is not surprising as it is the special case used to measure D-axis velocity as described above. Therefore, radar measurements taken at non-zero azimuth angles must be used to obtain the fully resolve three-dimensional ambient velocity vector. Furthermore, small azimuth angles will magnify errors in the other measured values.

The inverse of the NED-to-FPD coordinate transformation provides the means to solve for the measured wind vector in the Earth-fixed frame:

$$\dot{\overrightarrow{NED}} = [\boldsymbol{H}]^{-1}\dot{\overrightarrow{FPD}}$$

With the radar measured velocity vector represented in the FPD and NED frames, the wind speed is simply the magnitude of the horizontal components:

$$V_w = \sqrt{\dot{N}^2 + \dot{E}^2} = \sqrt{\dot{F}^2 + \dot{P}^2}$$

By taking the ratio of the North and East components, it follows that:

$$\tan\gamma = \frac{-\dot{E}}{-\dot{N}}$$

The wind direction (γ) can be unambiguously solved for using a quadrant-aware inverse tangent function (e.g. atan2).

The wind speed and direction can then be computed based on radar measurements at all non-zero azimuth angles. Radar range gates are mapped to altitude bins and samples are computed for all of the data in the recorded data file. A mean and standard deviation are then found for each altitude. The result is a set of plots showing reported and measured wind speeds and directions versus altitude.

3.3 Analysis Results

While post-processing recorded data files, radar velocity (Doppler) measurements and the results of the CONVEX algorithm are computed. These velocities represent the wind speed and precipitation rate as observed by the radar. Radar velocity measurements can only be made where there is sufficient reflectivity to receive a return signal. In general, no returns are received from above a certain altitude, likely due to being beyond the cloud tops. The minimum range of the radar also prevents taking measurements below about 3,000 feet in altitude.

3.3.1 Conventions

As a sign convention, positive velocity is defined for motion toward the radar (i.e. increased frequency Doppler shift) in the radial direction ($-V_R$). Likewise, a positive vertical velocity indicates motion from lower elevation angles to higher elevation angles (V_V). This would be equivalent to "up" or "skyward" relative to an aircraft. As discussed above, for the test configuration, this is for motion aligned with the longitudinal axis of the van moving from the back of the van toward the front of the van.

3.3.2 Qualitative Assessment Results

All measurement data was sampled while post-processing recorded radar data files. Direct radial velocity and vertical velocity measurements are the result of signal processing algorithms. It is important to recall that the purpose of this analysis is to validate the algorithms and not the radar itself (i.e. the radar has already been verified to provide accurate measurements). Where available, the velocity measurements are compared to the reported winds which are available from the surface to high altitudes.

3.3.2.1 *Velocity Results*

Radar velocity measurements are mapped into discrete color bins for displaying on plan position indicator (PPI) plot providing a view similar to a pilot cockpit display. The angular dimension is azimuth angle and the radial dimension is range. The range rings represent one kilometer graduations. For the test configuration, the radial dimension at zero azimuth angle is equivalent to altitude[4]. A constant altitude line would traverse horizontally across the plot. The figures included in this document represent a snapshot taken at the end of a sweep while post-processing a recorded data file.

The expected velocities computed from the reported wind conditions are used to produce a contour plot with an equivalent colormap. The contour is displayed in a PPI configuration for easy comparison to the measured data. Bilinear interpolation is used to fill in the contour between reported wind data points.

Because measurements were taken during the winter months, it is assumed that very little convective motion was occurring and observed vertical motion was due to precipitation. Since NOAA reported wind conditions provide only horizontal wind information, an assumption about vertical motion must be made. Because data was collected during precipitation events, a nominal rain fall rate of 10 miles per hour is

[4] NASA Langley is only a few meters above sea level

assumed at altitudes of 6,000 feet and below[5]. Above 6,000 feet altitude, it is assumed that vertical motion is negligible[6].

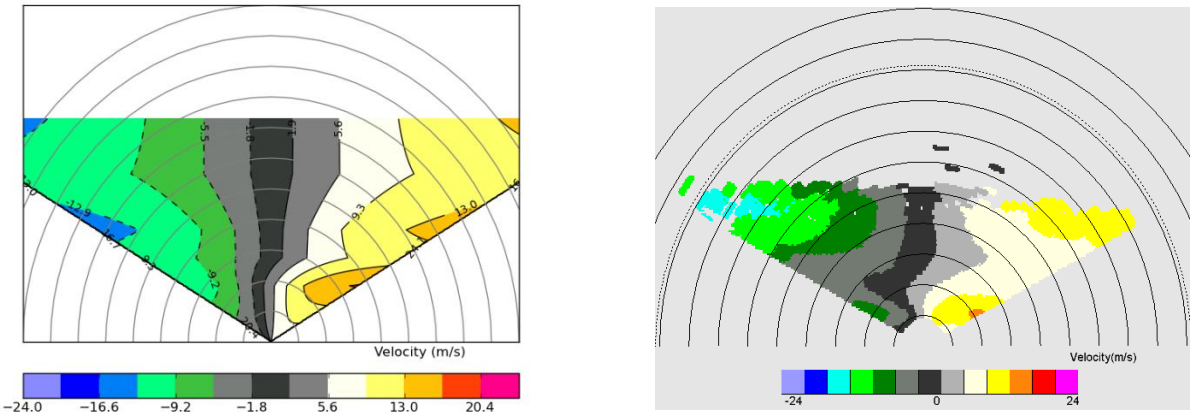

Figure 2: Velocity PPI Comparison, 2/8/2013, 160749, El 0^0, Van 30^0

Notice the region of black (indicating zero velocity) extends vertically at zero azimuth angle. This is as expected for a scan with a zero tilt angle as winds are orthogonal to the radar line-of-sight and do not contribute to the velocity measurement. However, precipitation is directly measurable at zero scan angles since the velocity is parallel to the radar line-of-sight. The shift in the black region to non-zero azimuth angles at close range (i.e. lower altitudes) shows that precipitation is occurring at lower altitudes but not at higher altitudes.

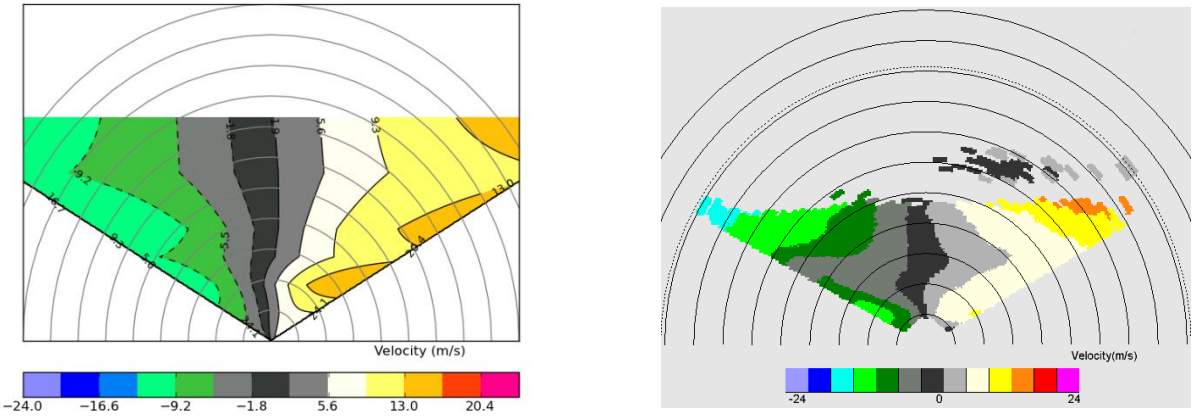

Figure 3: Velocity PPI Comparison, 2/8/2013, 160749, El -15^0 , Van 30^0

Velocity measurements are predominately positive at positive azimuth angles indicating that the antenna is scanning into the wind. Likewise, velocity measurements are predominately negative at negative azimuth

[5] For the recorded data used, measured reflectivity shows what appears to be a melting layer at roughly between 6,000 – 9,000 feet.

[6] Average velocity measurements along the vertical axis made during the quantitative analysis confirm this assumption.

angles indicating that the antenna is scanning away from the wind.

3.3.2.2 *CONVEX Algorithm Results*

Similar PPI contour plots are generated for the CONVEX algorithm results. Because the algorithm results in a velocity defined as perpendicular to the scan plane, it is not expected to vary with azimuth angle for a uniform wind field. It is expected to vary with altitude as the wind changes direction and speed as a function of altitude.

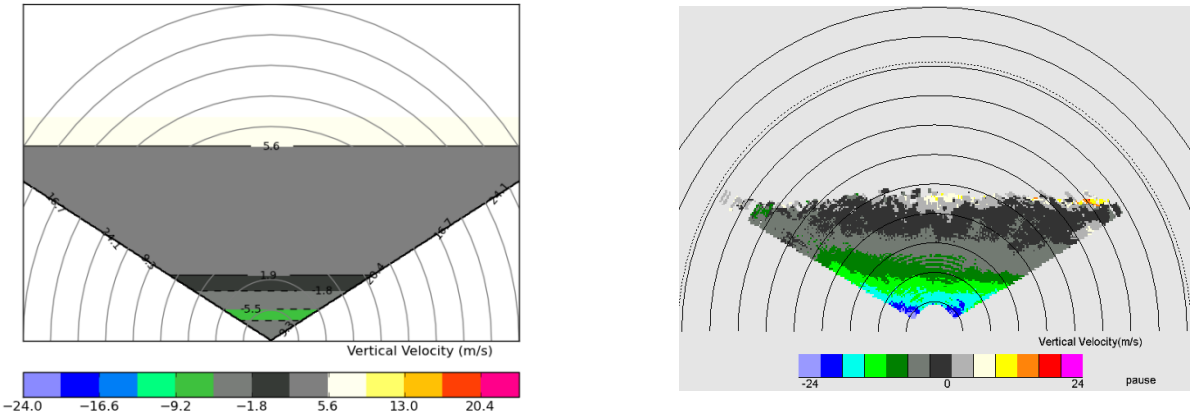

Figure 4: CONVEX Algorithm Velocity PPI Comparison, 2/8/2013, 160749, Van 30^{0} [7]

Notice the horizontal bands in the expected results. In general, velocity does not change with azimuth angle but does vary with altitude as expected. However, there are some variations in the measured CONVEX algorithm velocity at a given altitude (horizontal slice) at different azimuth angles. This is because the wind field is not uniform and varies in space and time. The NOAA reported winds represent an average at a given altitude, whereas the radar measurements are discrete samples.

An analysis was done for the results of the CONVEX algorithm calculation. The results from the algorithm were used to assess how well the resulting values compared to the truth data recorded from the NOAA site. This analysis reorganized vertical velocity estimates into 50 meter bins in altitude. The mean and the standard deviation of the CONVEX algorithm values was calculated for each 50 meter altitude bin. The results were compared to the truth data. To do a direct comparison the truth data was rotated into van coordinates. The following graphs show the comparisons. The blue line on each graph is the calculated mean and the black lines are the standard deviations at each altitude. The red and green lines are the truth data. The red lines are the truth data from the NOAA site at Norfolk International Airport (ORF). The first figure is from data recorded on February 8, 2013. This day included rain and the overcast cloud layer starting at about 500 feet and extending up to about 16000 to 17000 feet. Also the freezing layer was at about 6000 feet. The second figure was from data recorded on February 26, 2013. On this day light rain occurred and an overcast cloud layer started just below 5000 feet and extended up to about 23000 feet. The freezing layer was near 9000 ft. Also on the second figure the truth data from the NOAA site at Richmond International Airport (RIC) has been added for comparison.

[7] Because the operational purpose of the CONVEX algorithm is to estimate vertical velocity, the PPI displays for the algorithm results are labeled “vertical velocity.”

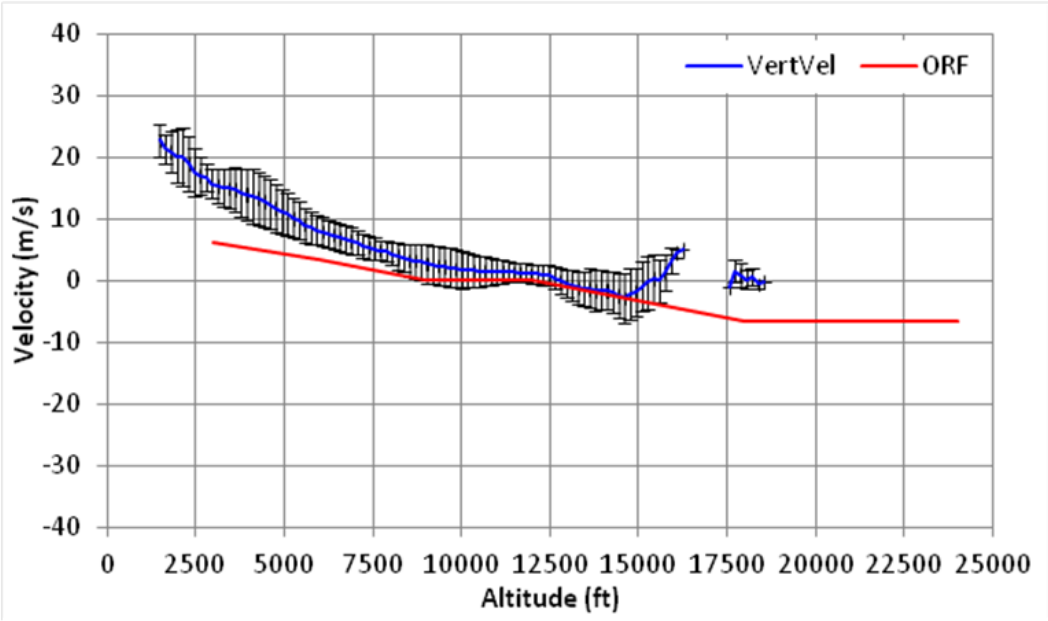

Figure 5: CONVEX Algorithm Velocity Comparison, 02/08/2013, 160749, Van 30^{o}

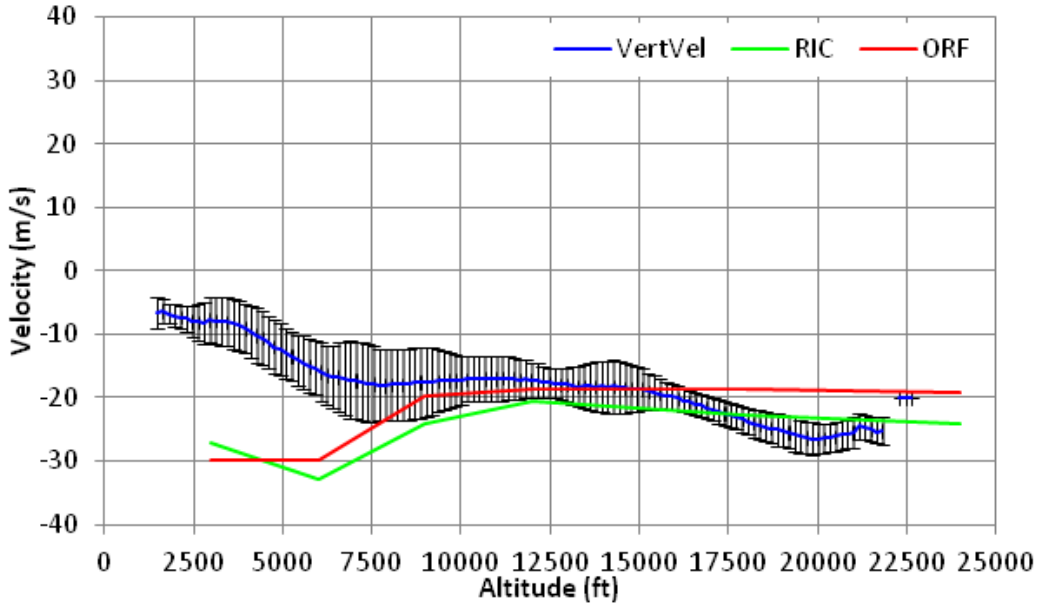

Figure 6: CONVEX Algorithm Velocity Comparison, 02/26/2013, 185057, Van 0^{o}

A more comprehansive set of results are avialable in the appendices. Appendix B provides additonal PPI contour plot comparisons. Appendix C provides additional altitude profile comparisons.

3.3.3 Quantitative Analysis Results

While post-processing recorded data files, radar velocity measurements are used to compute wind speed and direction samples at various scan angles (φ) for both tilt angles (θ) and all range bins for the duration of the data file. The samples are grouped by altitude and used to compute a mean and standard deviation at

each altitude bin. Standard line plots of mean wind speed and direction (with 1-σ error bars) versus altitude are generated.

Due to FFT processing and a fixed radar PRF, velocity aliasing can occur for sufficiently high wind speeds at certain radar orientations. For simplicity, aliased velocity data is discarded. Likewise, due to the coordinate transformation singularity at zero scan angle, measurement data for small azimuth angles ($\varphi < 15^0$) is also discarded – with the exception of the special case described above for obtaining vertical velocity.

For comparison, line plots of reported wind speed and direction versus altitude are overlaid with the measured data. Multiple sets of reported conditions (from different locations and/or times) may be included.

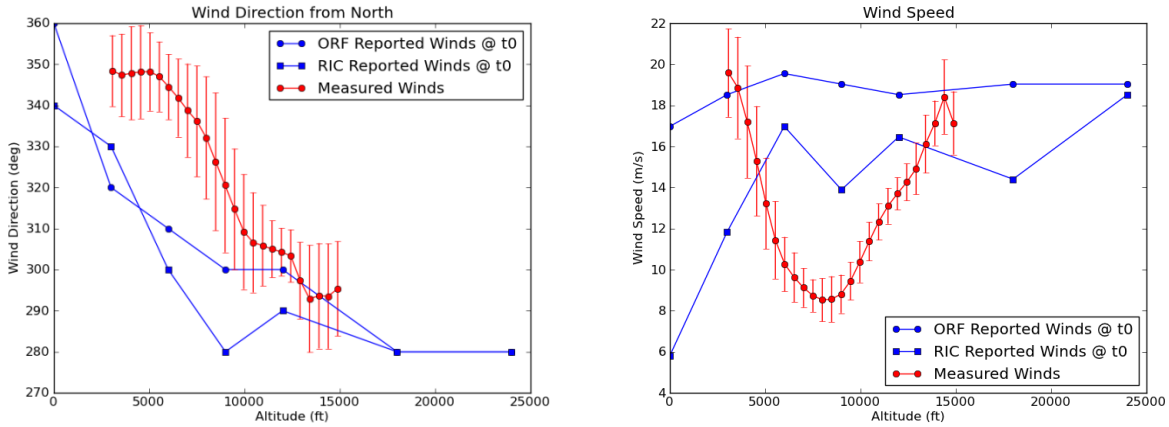

Figure 7: Quantitative Wind Comparison, 2/8/2013, 160749, Van 30^0

A more comprehansive set of results are provided in Appendix D.

3.3.4 Turning Van Scenario

During the case in which the van was driven around in a circle, data recording was started and stopped with the van facing to the North. Two full rotations were completed in just over two minutes twenty seconds. For the analysis, the following turn rate is assumed: 2 x 360^0 ÷ 140.71 sec = 5.12 deg/sec. It is also assumed that translation motion is negligible.

Because the quantitative analysis approach relies on the CONVEX algorithm, it is important to understand the limitations of the algorithm in this unusual scenario. The algorithm assumes that the two scans used (for the 2-bar process) are co-planer except for the known elevation difference. In other words, it relies on the radar automatic tilt compensation to remove aircraft roll angle. In the test configuration, turning the van is equivalent to a constant uncompensated roll rate. Consequently, the CONVEX calculation is only valid near the beginning of a sweep (just after turn-around) when the angle between the two sweep planes is sufficiently small. Therefore, all measurements beyond small azimuth angles (> 15^0) from beginning of sweep are discarded.

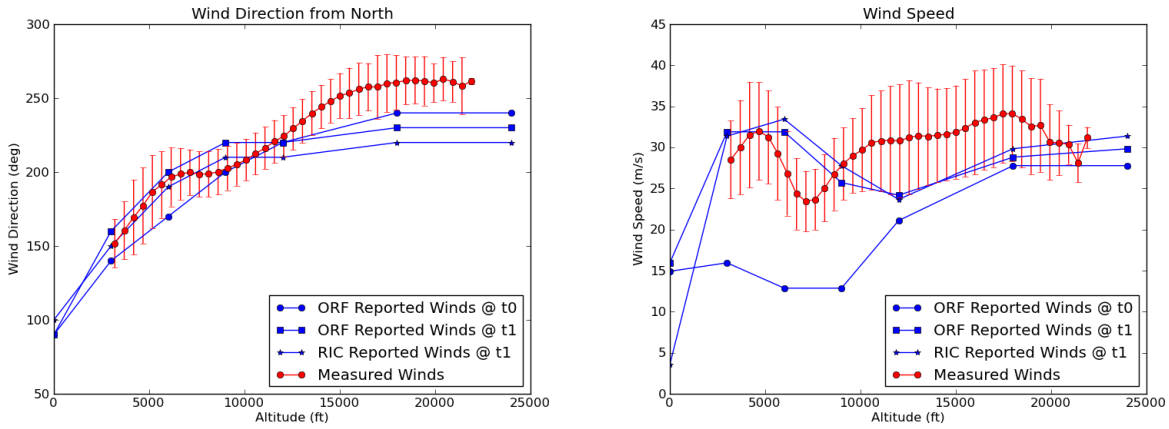

Figure 8: Quantitative Wind Comparison, 2/26/2013, 204900, Van Turning

4 Flight Test Assessment

A Doppler, weather radar was operated under normal flight conditions utilizing the HU-25 Falcon aircraft at NASA Langley Research Center. Test sorties were flown on days with rain storms in the mid-Atlantic region that showed signs of convective activity. Radar reflectivity and velocity measurements were taken while flying toward convective cells at various altitudes. The objectives for the flight tests were to collect airborne data from a moving platform to evaluate the performance of the complete algorithm employing the three-bar sequence. This extends the assessment beyond the ground test results which only evaluate the two-bar sequence.

4.1 Flight Test Description

A commercial airborne Doppler weather radar was installed on the Langley HU-25 Falcon aircraft and operated following normal flight operations procedures. The weather mode automatically adjusts antenna tilt depending on altitude and produces a composite view for the cockpit Multi-Function Display (MFD) using two different tilt angles. During test runs, the aircraft was flown under Visual flight rules (VFR) conditions. The MFD and visual inspection were used to locate convective cells for data collection. Each data collection run consisted of flying directly toward a cell from thirty to forty nautical miles away and approaching as close as the pilot-in-command deemed safe. Runs were completed at altitudes of 20,000, 25,000, and 30,000 feet.

The antenna was mounted in the standard configuration behind the radome on the forward bulkhead oriented forward with positive azimuth in the starboard direction. Likewise, antenna tilt angles were oriented so that negative angles were toward the ground. The radar automatically compensates for aircraft pitch and roll so that the radar beam sweeps through a flat plane at the commanded tilt. The CONVEX algorithm computes a component of the velocity vector perpendicular to the radar scan plane at zero elevation angle. In this flight test orientation, the algorithm result is vertical wind speed from the ground up.

Figure 9: NASA Langley HU-25 Falcon Aircraft

Data recording equipment was rack mounted in the aircraft cabin. This equipment was used to record radar data and aircraft state information. Additionally, a video recorder was mounted in the cockpit facing forward out the windscreen to collect visual data.

The radar transceiver was set up with a range bin size of 300 meters. Three hundred twenty-one range bins of data were collected. The 321 range bins resulted in just over 96000 meters of radar data. The antenna had a beam width of 5 degrees in both azimuth and elevation. The scans of the antenna in azimuth were from -60 degrees to +60 degrees. Since the platform is moving during the flight test, the three-bar equations are used to make the vertical velocity calculations described in Section 2, CONVEX Algorithm.

About 320 minutes of radar data was collected over three separate sorties. A summary of all the data collected is in a table in Appendix A.

Figure 10: Data Recording Equipment

4.2 Analysis Approach

Analysis of the recorded radar data was completed using the same post-processing tool as for the ground test. However, the ambient conditions are not know, consequently a direct comparison cannot be made. The following assessment of the flight test data is the first set of data that demonstrates the CONVEX algorithm operating in an airborne environment.

4.3 Flight Test Results

While post-processing recorded data files, radar velocity (Doppler) measurements and the results of the CONVEX algorithm are computed. After compensating for aircraft motion, these velocities represent the wind speed as observed by the radar. Radar velocity, both radial and vertical, measurements can only be made where there is sufficient reflectivity to receive a return signal. All measurement data was sampled while post-processing recorded radar data files. Direct radial velocity and vertical velocity measurements are the result of signal processing algorithms. It is important to recall that the purpose of this analysis is to validate the algorithms and not the radar itself (i.e. it is assumed that the radar provides accurate measurement data). The calculations of the vertical velocity with this flight data account for the translations and rotations of the aircraft as described above in section 2.3 Compensating for Platform Rotation.

Figure 11: Convective Cloud Measured During Research Flight 1 on 10 September 2014

The algorithm description and ground test results utilize a tilt difference of 15 degrees, however the airborne radar system on the HU-20 Falcon produced a two-bar tilt sequence with a tilt difference of only two degrees. This quantity was accepted in order to operate within the existing hardware paradigm, however it is less than desirable because the CONVEX algorithm is sensitive to the velocity differences between the two sweeps which is driven by their angular separation. Most antenna beam widths are 4 or 5 degrees. Therefore, a difference in two degrees of tilt between two sweeps means the measurements are not completely independent of each other. The two degree difference in the tilt angles resulted in quite small differences in altitude at close ranges to the aircraft. For instance, at a range of 1 km, the altitude difference between the two sweeps is only 35 meters, whereas for a 15 degree tilt difference at the same range the altitude difference is about 270 meters. To get an equivalent 270 meter altitude difference with a 2 degree tilt difference, the returns would need to be located just beyond 7.5 km in range.

An alternating two-bar tilt pattern was continuously repeated which allowed for the use of the three-bar sequence algorithm as described above for the scan sequence and the alternate scan sequence. The three-bar sequence does develop a singularity directly in front of the aircraft due to the little or no change in

azimuth angle between the two common tilt sweeps. Therefore, the two-bar sequence is used for small azimuth angles directly in front of the aircraft. When using the two-bar sequence, the radial velocity measurements between the two sweeps can be nearly the same, especially if there is overlapping of the beam and the two samples are not independent. If the tilt difference is large enough for independent samples, the resulting vertical velocity estimated by the two-bar sequence algorithm can be as accurate as that estimated by the three-bar sequence algorithm.

4.3.1 Conventions

As a sign convention, the flight program used the same sign convention as used in the ground test. That is a sign convention of positive velocity is defined for motion toward the radar (i.e. increased frequency Doppler shift) in the radial direction ($-V_R$). Likewise, a positive vertical velocity indicates motion from lower elevation angles to higher elevation angles (V_V). This is equivalent to "up" or "skyward" relative to the aircraft.

4.3.2 Velocity Results

Radar return power and velocity measurements are mapped into discrete color bins for displaying on plan position indicator (PPI) plots providing a view similar to the cockpit MFD. The angular dimension is azimuth angle and the radial dimension is range. For the flight data, the maximum range was about 100 kilometers. The range rings represent five kilometer graduations.

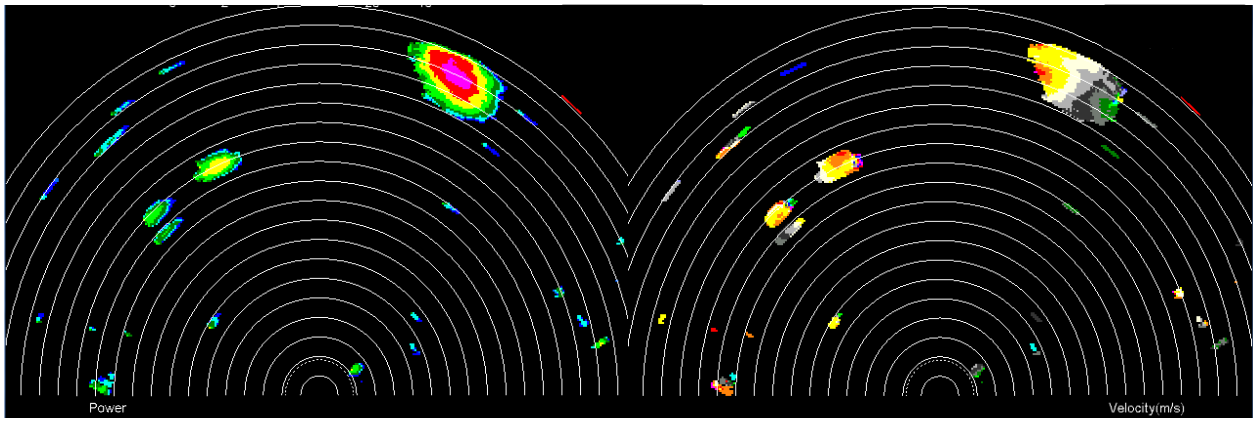

Figure 12: Example PPI Showing Power Relative to the Noise Floor (left) & Radial Velocity (right)

If the radial velocities result in Doppler frequencies which exceed the Nyquist frequency for the radar, then velocity aliasing can occur. This results in errors in the vertical velocity estimates produced by the CONVEX algorithm. The upper right portion of the large cell shows radial velocities from negative (purple) to positive (yellow) and back to negative (green) in close proximity; an indication of velocity aliasing. These radial velocity errors will contribute to the large errors in the vertical velocity estimates.

4.3.3 Vertical Velocity Results

The following example shows the same cell as above was encountered and the updraft measured. The cell is on the right at about +30 degrees azimuth and 80 to 95 kilometers in range from the aircraft. At that range, the difference in altitude between the two tilt angles is around 2.7 km to 3.3km. This difference in altitude is near the maximum desirable to reduce the likelihood of spatial variability in the vertical velocities. Even with this altitude separation, the two measurements are from radar beams which overlap, meaning they are not entirely independent measurements. The image below shows the results of the

CONVEX vertical velocity algorithm. The dark gray color represents negative or downward vertical velocity where the light grey, white, and magenta colors represent the positive vertical velocities.

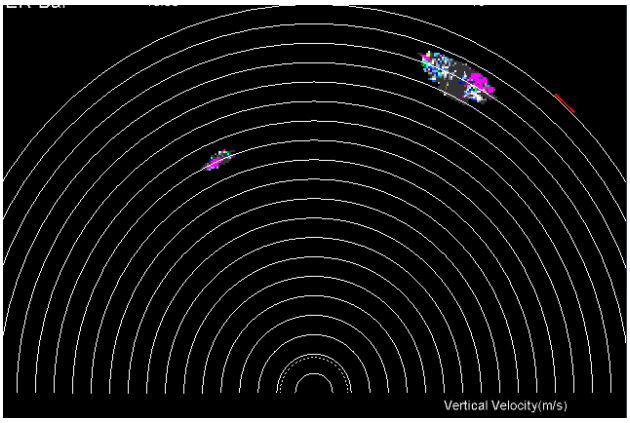

Figure 13: Example PPI Showing Results of the CONVEX Algorithm (Vertical Velocity)

As the position of the cell moves closer to the aircraft and the cell grows larger a second cell nearby develops with some relatively high power as well. The cell is now about 70 km to 95 km from the aircraft. At this nearer range, the difference in altitude between the two sweeps is 2.4 km at the near edge of the cell to 3.3 km at the far edge of the cell. The image on the left depicts the received power relative the noise floor, and the image on the right depicts the power with the vertical velocity output overlaid on top. This illustrates the spatial correlation between the core of the cells (as indicated by strong echoes) and evidence of convection (as indicated by vertical velocities estimated by the CONVEX algorithm). The results show positive vertical velocity for both areas of strong radar return power.

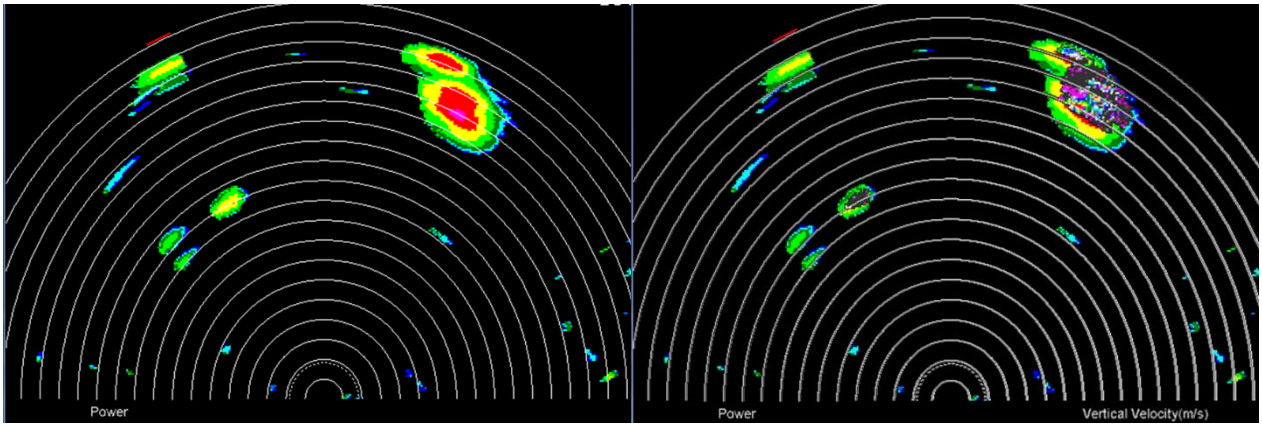

Figure 14: Example PPI Showing Power Relative to the Noise Floor (left) & Vertical Velocity Overlaid on the Power Display (right)

The uncertainties in the radial velocity measurements, the velocity aliasing, and the small angle difference between the two tilts contribute to errors in the resulting vertical velocity estimates making the flight test results less conclusive than the ground test results. Additionally, the actual values of vertical velocity cannot be validated because the airplane did not fly through the storms and measure actual vertical winds ("truth data"). A follow on flight test that measures the vertical winds will permit a more quantifiable assessment of how well the algorithm works under actual flight conditions. This would support a direct comparison similar to the ground tests comparisons described above. Nevertheless, the flight tests

demonstrated the CONVEX algorithm operating in real time on a moving airborne platform.

5 Conclusions and Future Work

A methodology for producing a measure of the convective wind field ahead of an aircraft using a modern, airborne, Doppler, weather radar is described and a working algorithm (CONVEX) implemented. Determining the location and magnitude of convective weather can provide pilots with awareness of convective activity in their vicinity. Awareness of areas of convection can improve aviation safety by providing a means of avoidance or departure guidance if hazardous conditions are encountered.

Ground and flight tests have been performed to validate a new convection (CONVEX) application for airborne weather radars. These tests utilized unmodified existing, commercial weather radars such as those currently flying on transport and regional jet aircraft. The new application does not require any changes to the existing hardware and exploits the existing scan strategies employed in modern weather radars for volumetric weather observations and ground clutter suppression, meaning that the method can be implemented in software only. The technique does rely upon good aircraft state data and is designed to only detect upward (skyward) blowing winds (not downward blowing winds – whose measurements would be complicated by the gravity induced motion of the wind-tracing hydrometeors).

The ground test results provide a qualitative and quantitative assessment of the algorithm performance, although from a stationary platform. The results of the ground tests show favorable agreement with the measured wind field. The flight test results provide a qualitative assessment of the algorithm performance operating in real time on a moving airborne platform. These results demonstrate how well the algorithm takes account of the linear and angular motion of the aircraft. The motion of the aircraft requires the algorithm to associate the same column of air from the three different sweeps. Overall, the flight test results show a reasonable correlation between the locations estimated to contain strong vertical velocities and the cores of convective storm cells.

While the flight testing perform so far is not conclusive, the CONVEX algorithm shows sufficiently encouraging performance to merit additional flight testing. To permit a more quantitative assessment of the results, a measure of the actual vertical winds must be available. This may be accomplish by flying through convective conditions and sampling the winds directly. Further testing the algorithm with larger tilt angle differences between the sweeps will significantly reduce the errors in the vertical velocity estimate. Likewise, reducing or compensating for radial velocity aliasing would improve the estimate.

Appendix A

Tabular summary of recorded radar data and reported weather conditions. The table has the date, the time and the direction of the van from each data recording. The rest of the columns are the conditions reported at Norfolk International Airport from NOAA on the wind speed and direction at different altitudes.

			NOAA Reported Wind Direction and Speed(deg@kts)				
Date	**Time**	**Van (deg) (true north)**	**3000 ft**	**6000 ft**	**9000 ft**	**12000 ft**	**18000 ft**
2/7/2013	203946	30	150 @ 17	240 @ 9	240 @ 14	240 @ 45	250 @ 58
2/7/2013	205635	30					
2/7/2013	210512	30					
2/7/2013	210744	30					
2/7/2013	210944	30					
2/8/2013	151223	30	320 @ 36	310 @ 38	300 @ 37	300 @ 36	280 @ 38
2/8/2013	151831	30					
2/8/2013	152619	30					
2/8/2013	153558	30					
2/8/2013	154650	30					
2/8/2013	160046	30					
2/8/2013	160749	30					
2/8/2013	165259	30					
2/8/2013	170057	30					
2/11/2013	201845	30	260 @ 45	260 @ 57	240 @ 53	240 @ 42	280 @ 70
2/13/2013	165359	30	160 @ 15	230 @ 46	250 @ 54	250 @ 59	260 @ 79
2/13/2013	214931	30	240 @ 24	260 @ 38	250 @ 55	250 @ 84	
2/13/2013	215526	30					
2/13/2013	215942	30					
2/19/2013	185548	30	210 @ 43	230 @ 57	220 @ 59	230 @ 66	240 @ 71
2/19/2013	190029	30					
2/19/2013	190349	30					
2/19/2013	190735	30					
2/19/2013	191053	30					
2/19/2013	191706	30					
2/19/2013	192106	30					
2/19/2013	201511	30	210 @ 47	230 @ 48	220 @ 62	230 @ 64	
2/19/2013	202216	30					
2/22/2013	154927	30	160 @ 09	250 @ 33	270 @ 38	270 @ 39	290 @ 57
2/22/2013	160755	30					
2/22/2013	161324	30					
2/26/2013	185057	0	140 @ 31	170 @ 25	200 @ 25	220 @ 41	240 @ 54
2/26/2013	185757	0					
2/26/2013	191303	0					
2/26/2013	192836	90					
2/26/2013	194045	90	160 @ 62	200 @ 62	220 @ 50	220 @ 47	230 @ 56
2/26/2013	195327	180					
2/26/2013	200258	130					
2/26/2013	201209	45					

2/26/2013	202611	225					
2/26/2013	204900	circular,start 0					
2/26/2013	205713	30					
2/26/2013	211930	30					
3/5/2013	213418	30	190 @16	240 @ 29	270 @ 41	270 @ 43	270 @ 43
3/5/2013	213913	30					
3/5/2013	215211	30					
3/5/2013	215437	30					
3/6/2013	211734	30	260 @ 27	290 @ 17	320 @ 12	330 @ 13	340 @ 18
3/6/2013	212734	30					

Tabular summary of recorded flight test data.

	Start Time	Stop Time	Altitude	Outside Air Temperature
ICF 4 September 2014				
Run 1	13:52:00		16,308 ft	-3 C
Run 2	14:10:10		15,289 ft	-2 C
Run 3	14:15:40		15,340 ft	-2 C
Research Flight 1 10 September 2014				
Run 1	13:23:10	13:25:40	30,000 ft	-34 C
Run 2	13:33:15	13:36:20	30,000 ft	-34 C
Run 3	13:48:00	13:50:00	25,000 ft	-23 C
Run 4	14:01:00	14:04:50	25,000 ft	-23 C
Run 5	14:14:30	14:20:20	20,000 ft	-10 C
Research Flight 2 24 September 2014				
Run 1	12:55:25	12:57:45	35,000 ft	-46 C

Appendix B

Graphical comparison of radial velocity and CONVEX algorithm velocity PPI displays (qualitative assessment results) from ground testing.

(Note: because the operational purpose of the CONVEX algorithm is to estimate vertical velocity, the PPI displays for the algorithm results are labeled "vertical velocity.")

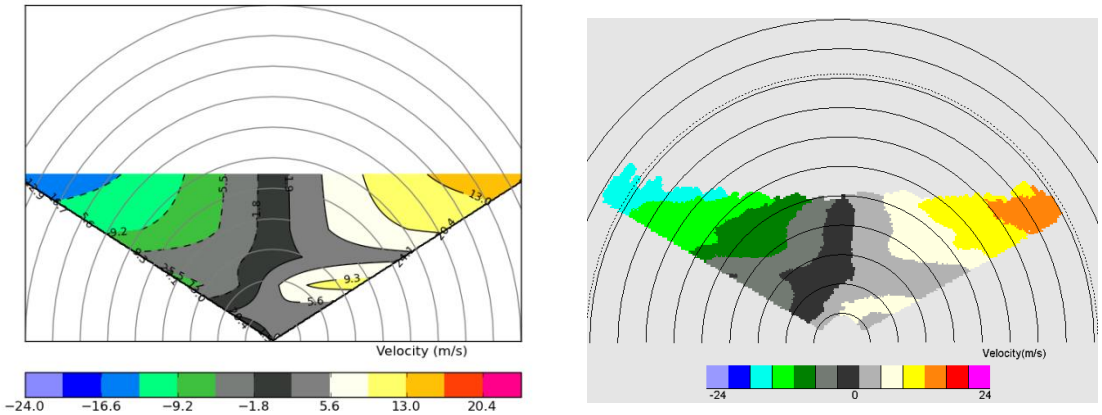

Figure 15: Velocity PPI Comparison, 2/19/2013, 185548, El 0^0, Van 30^0

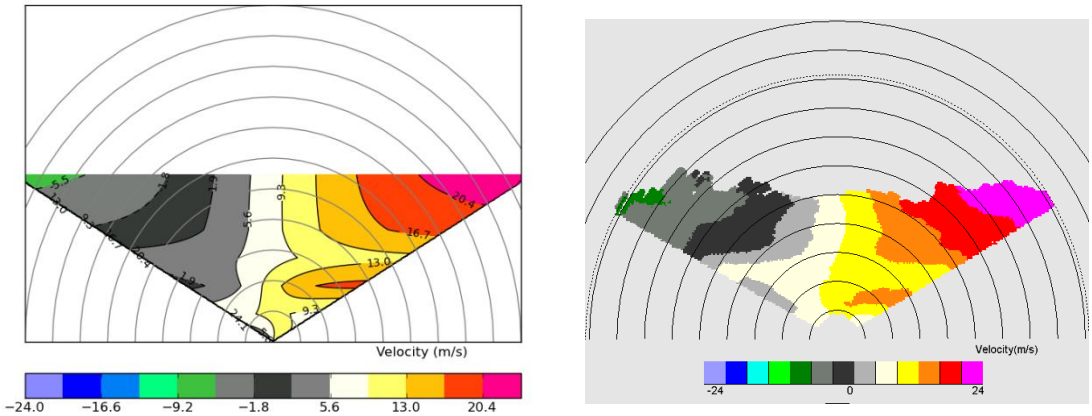

Figure 16: Velocity PPI Comparison, 2/19/2013, 185548, El -15^0 , Van 30^0

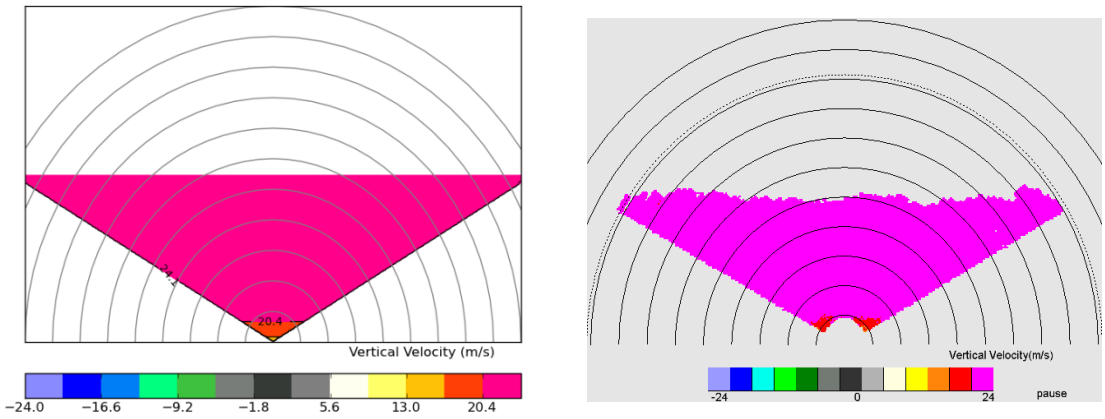

Figure 17: CONVEX Algorithm Velocity PPI Comparison, 2/19/2013, 185548, Van 0^0

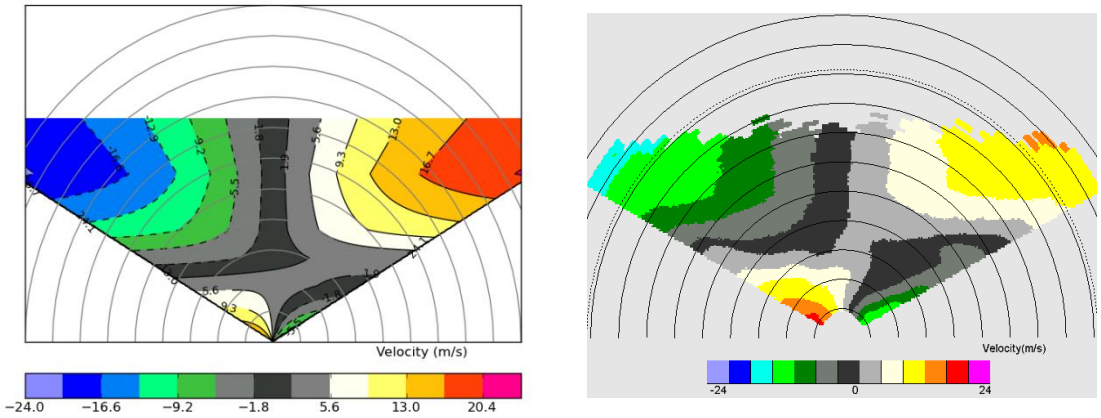

Figure 18: Velocity PPI Comparison, 2/26/2013, 185057, El 0^0 , Van 0^0

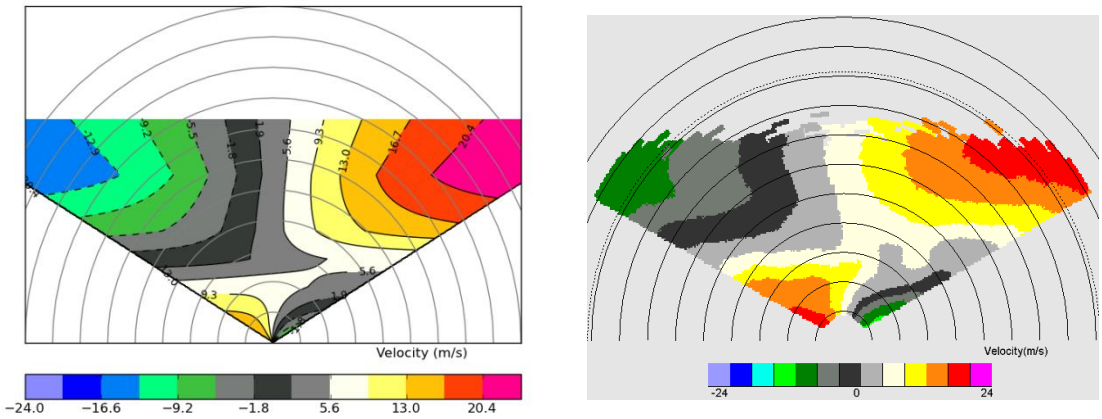

Figure 19: Velocity PPI Comparison, 2/26/2013, 185057, El -15^0 , Van 0^0

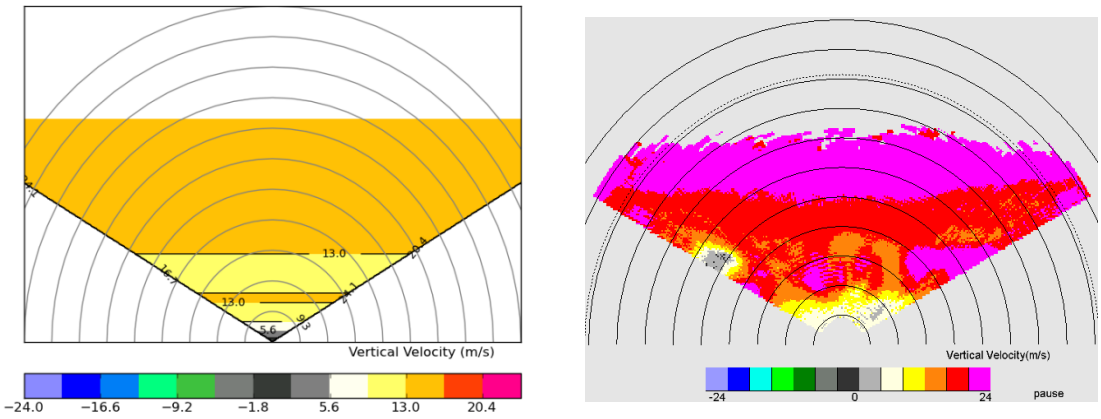

Figure 20: CONVEX Algorithm Velocity PPI Comparison, 2/26/2013, 185057, Van 0^0

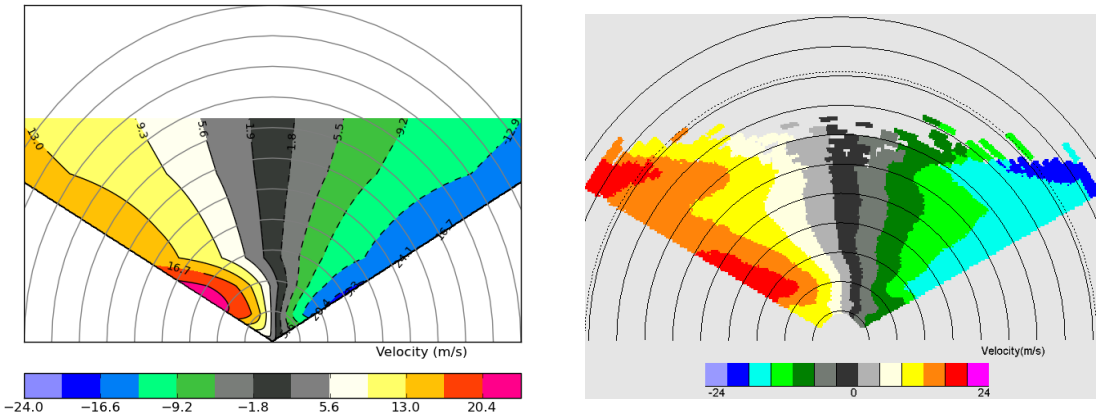

Figure 21: Velocity PPI Comparison, 2/26/2013, 192836, El 0^0 , Van 90^0

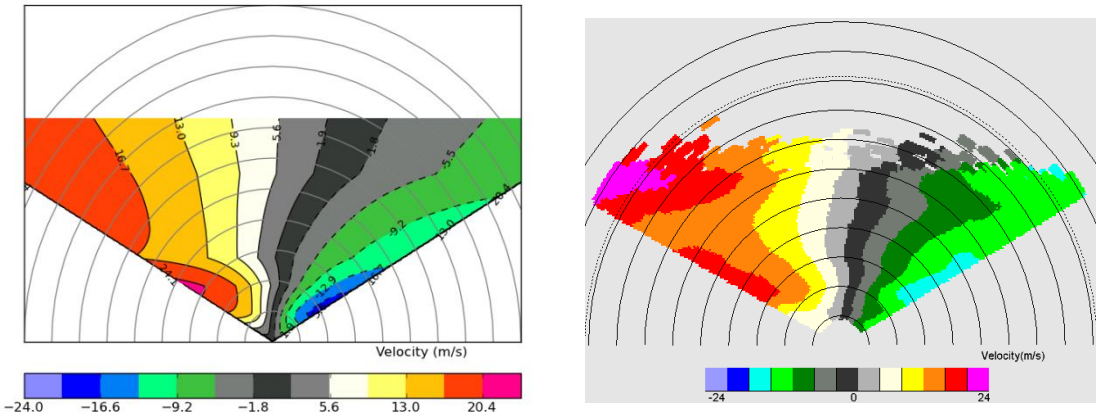

Figure 22: Velocity PPI Comparison, 2/26/2013, 192836, El -15^0 , Van 90^0

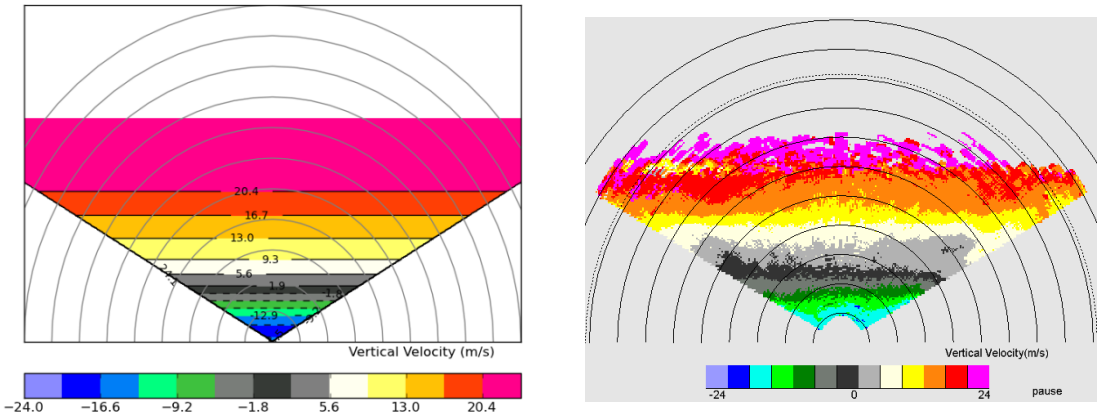

Figure 23: CONVEX Algorithm Velocity PPI Comparison, 2/26/2013, 192836, Van 90^0

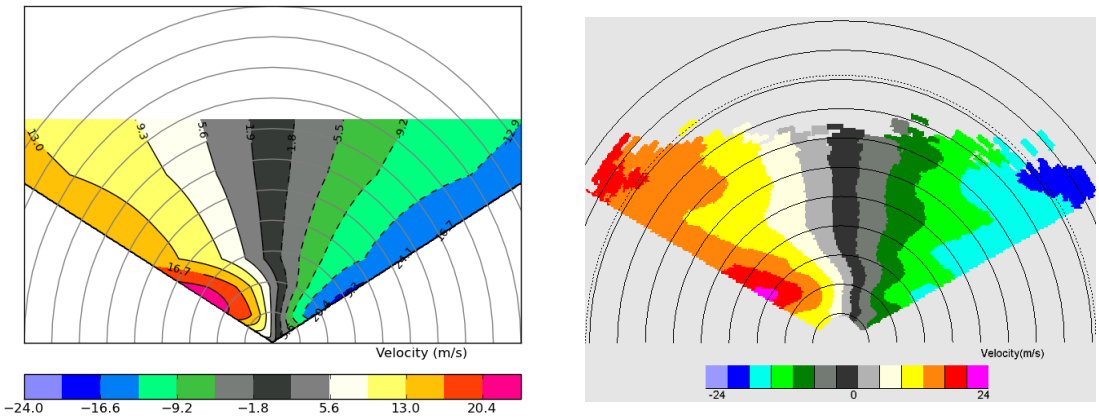

Figure 24: Velocity PPI Comparison, 2/26/2013, 194045, El 0^0 , Van 90^0

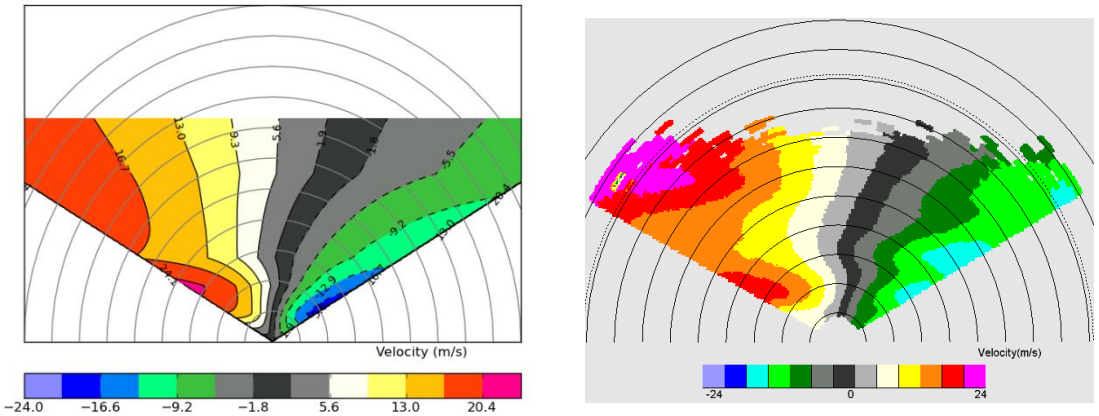

Figure 25: Velocity PPI Comparison, 2/26/2013, 194045, El -15^0 , Van 90^0

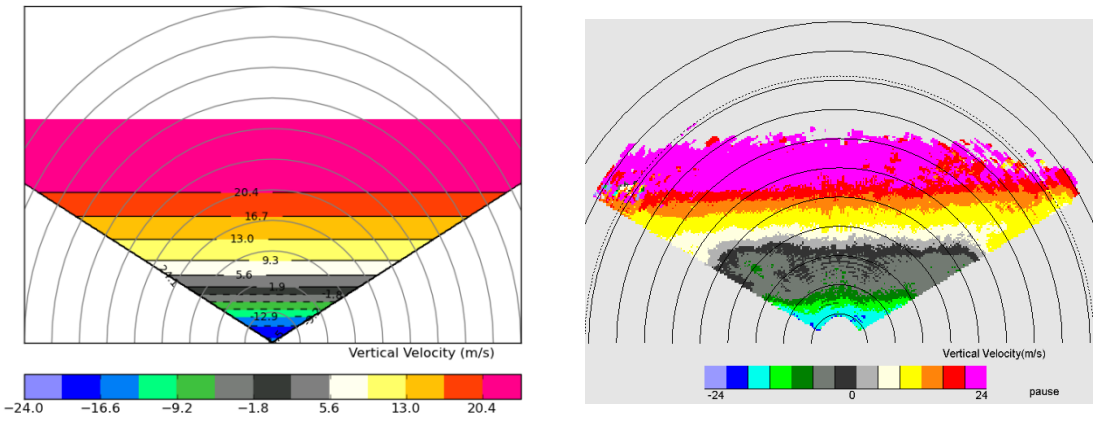

Figure 26: CONVEX Algorithm Velocity PPI Comparison, 2/26/2013, 194045, Van 90^0

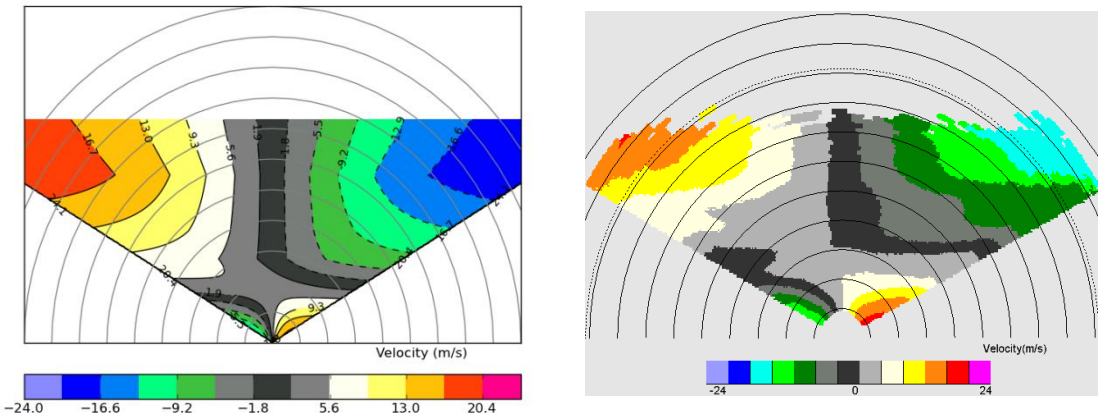

Figure 27: Velocity PPI Comparison, 2/26/2013, 195327, El 0^0 , Van 180^0

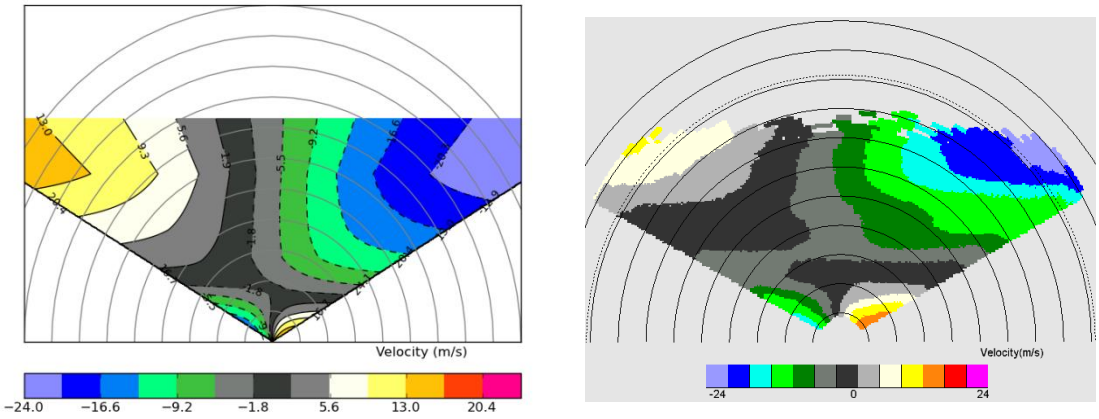

Figure 28: Velocity PPI Comparison, 2/26/2013, 195327, El -15^0 , Van 180^0

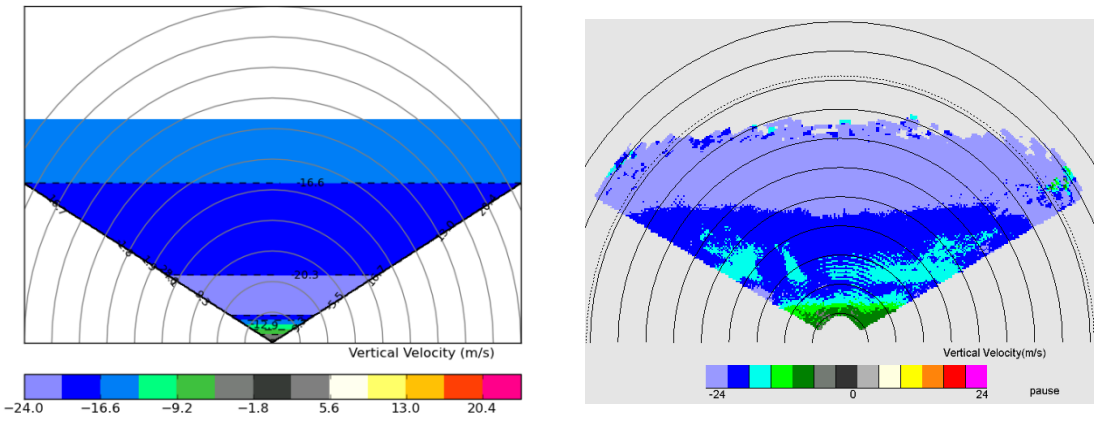

Figure 29: CONVEX Algorithm Velocity PPI Comparison, 2/26/2013, 195327, Van 180^0

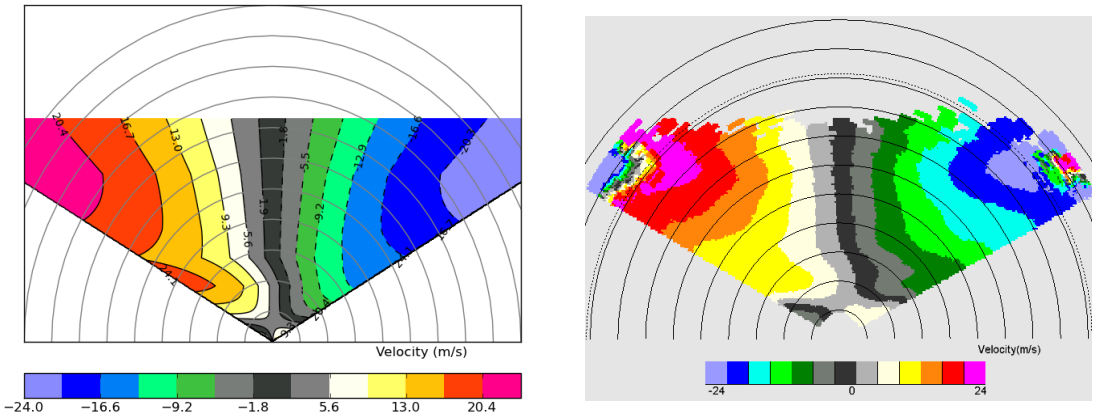

Figure 30: Velocity PPI Comparison, 2/26/2013, 200258, El 0^0 , Van 130^0

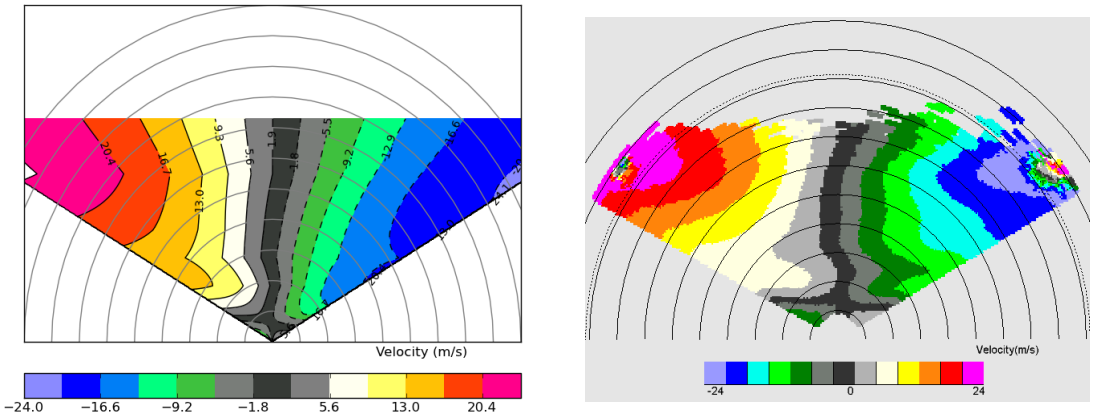

Figure 31: Velocity PPI Comparison, 2/26/2013, 200258, El -15^0 , Van 130^0

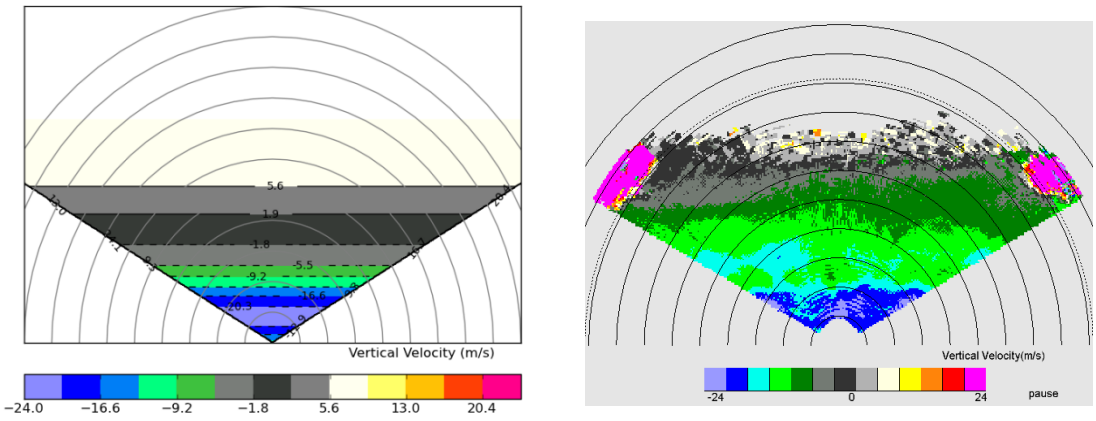

Figure 32: CONVEX Algorithm Velocity PPI Comparison, 2/26/2013, 200258, Van 130^0

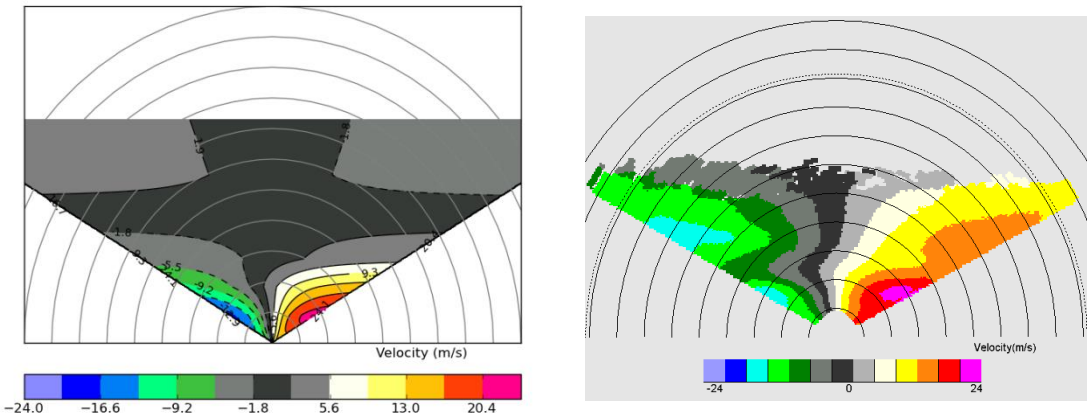

Figure 33: Velocity PPI Comparison, 2/26/2013, 202611, El 0^0 , Van 225^0

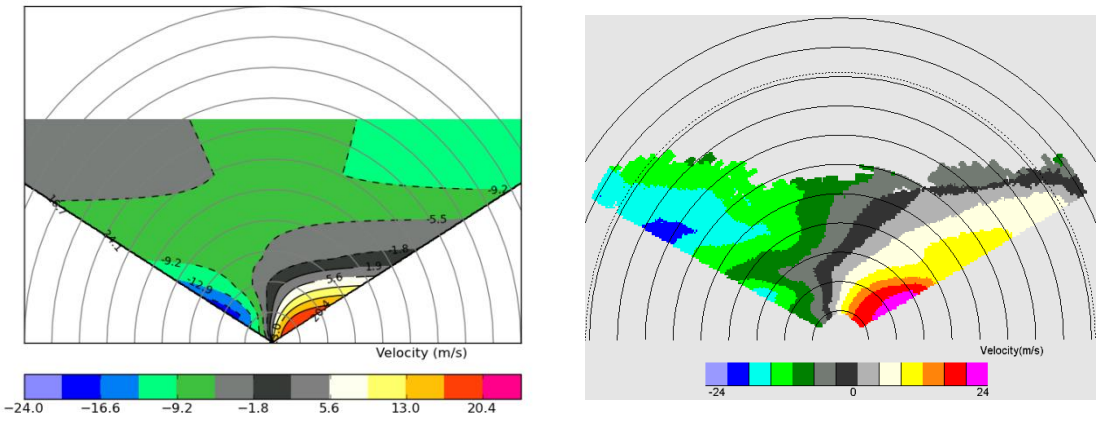

Figure 34: Velocity PPI Comparison, 2/26/2013, 202611, El -15^0 , Van 225^0

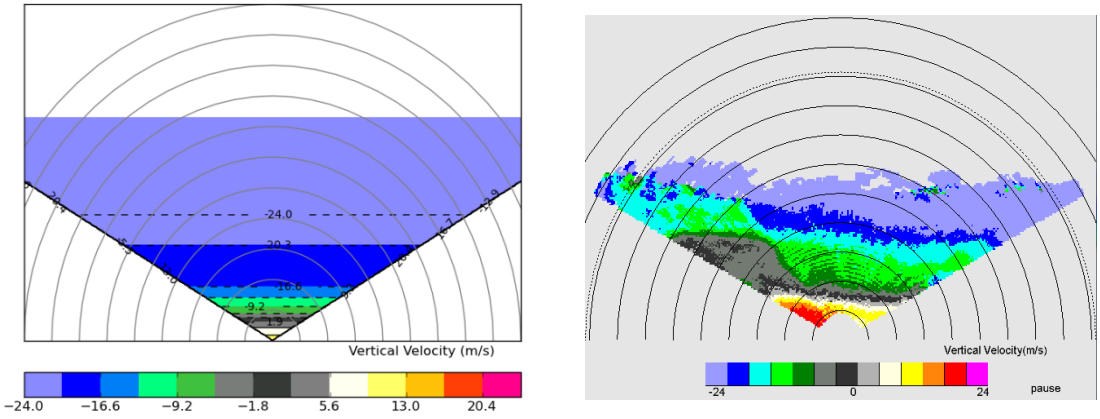

Figure 35: CONVEX Algorithm Velocity PPI Comparison, 2/26/2013, 202611, Van 225^0

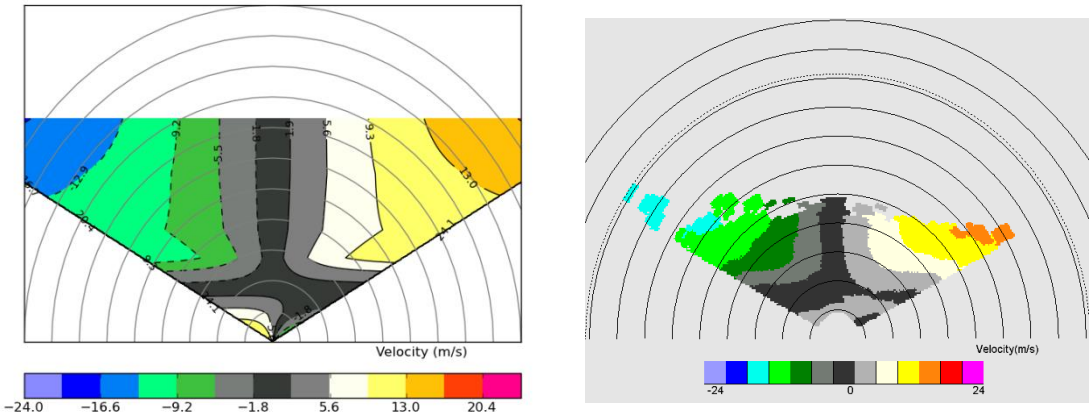

Figure 36: Velocity PPI Comparison, 3/5/2013, 213913, El 0^0 , Van 30^0

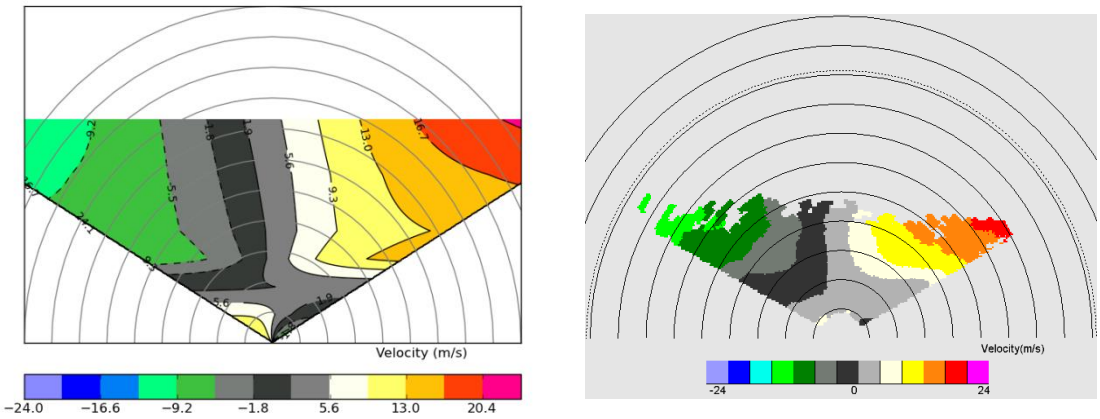

Figure 37: Velocity PPI Comparison, 3/5/2013, 213913, El -15^0 , Van 30^0

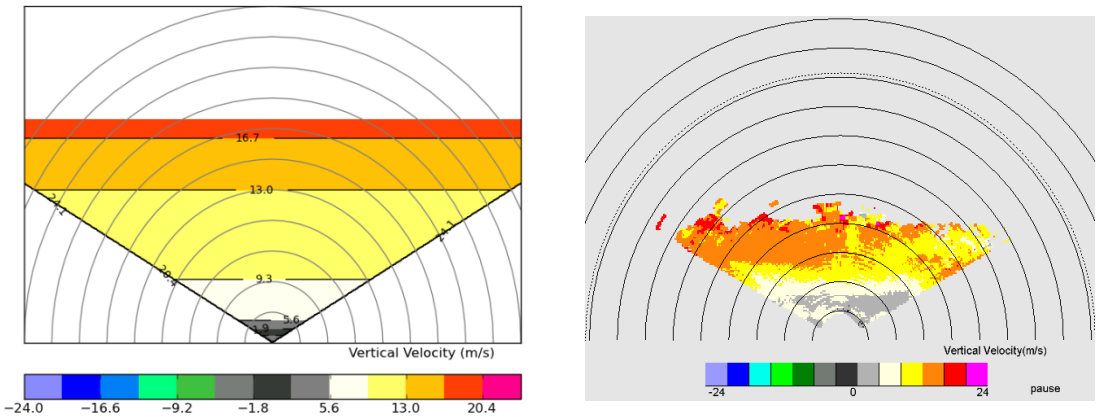

Figure 38: CONVEX Algorithm Velocity PPI Comparison, 3/5/2013, 213913, Van 30^0

Appendix C

Graphs of Mean and standard deviation of the vertical velocity. These graphs show the results from the different van directions from Feb 26, 2013.

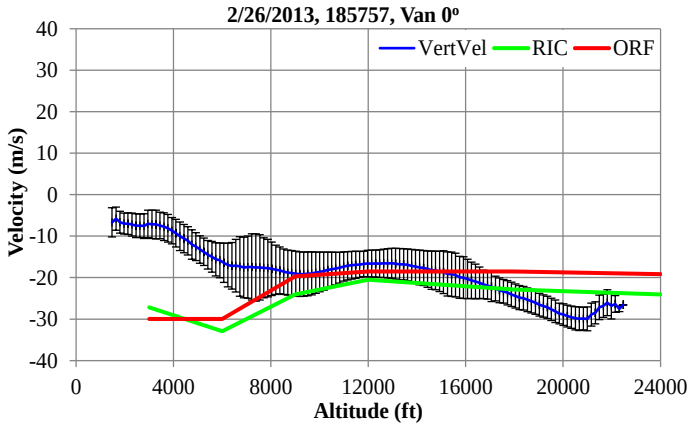

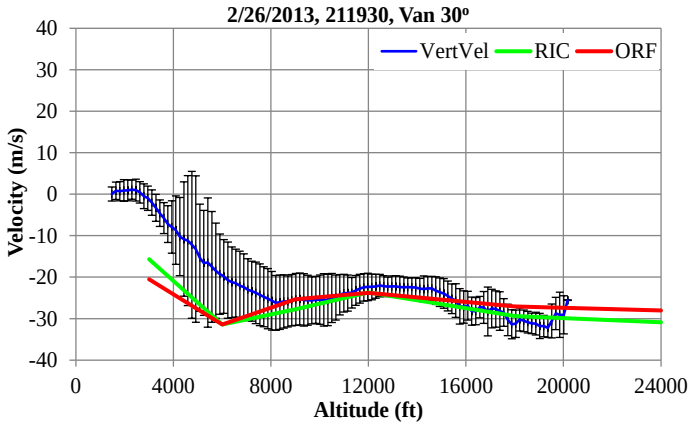

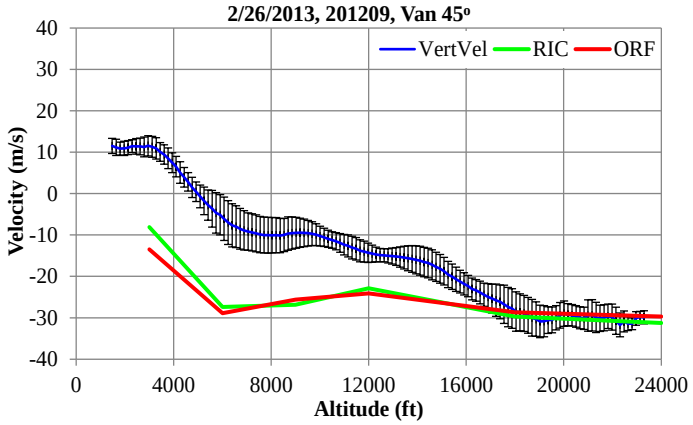

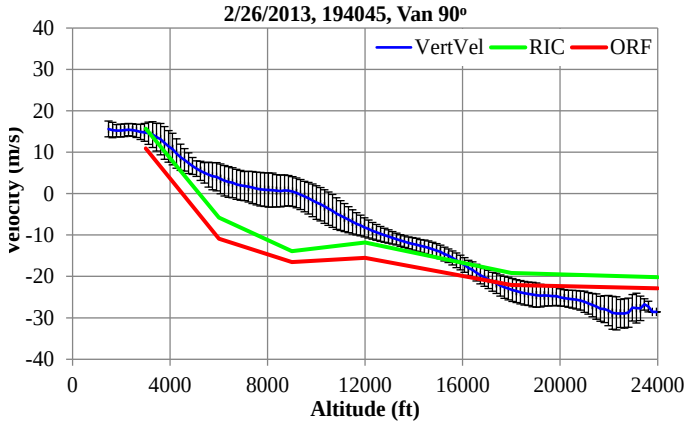

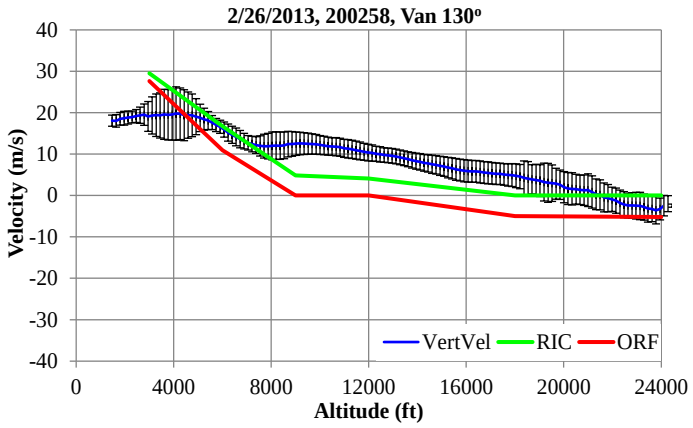

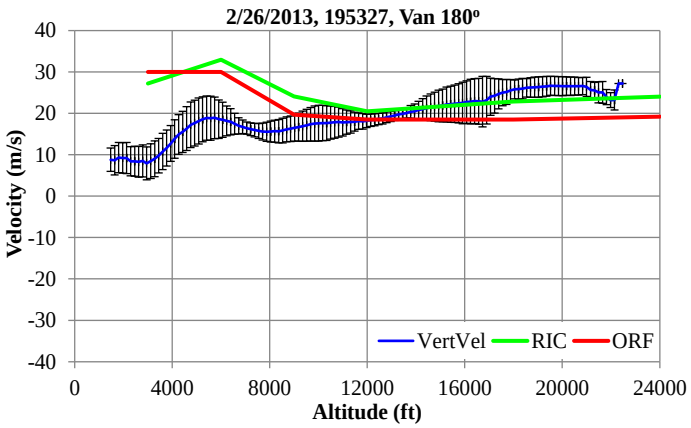

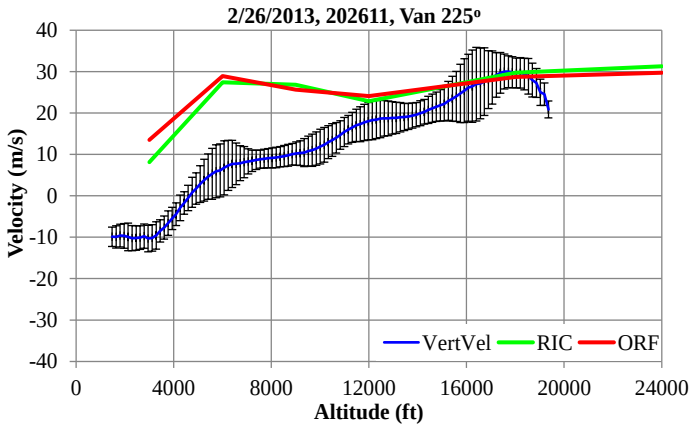
2/26/2013, 202611, Van 225°
Velocity (m/s)
Altitude (ft)
VertVel
RIC
ORF

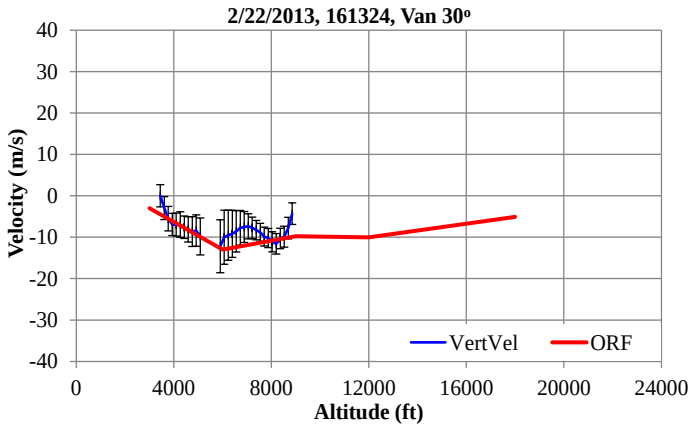
2/22/2013, 161324, Van 30°
Velocity (m/s)
Altitude (ft)
VertVel
ORF

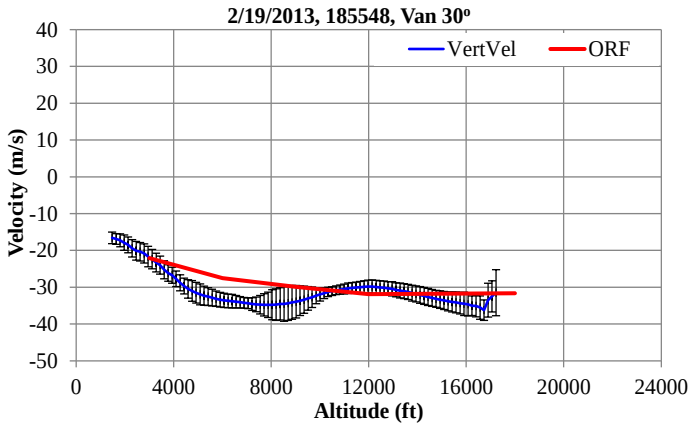
2/19/2013, 185548, Van 30°
Velocity (m/s)
Altitude (ft)
VertVel
ORF

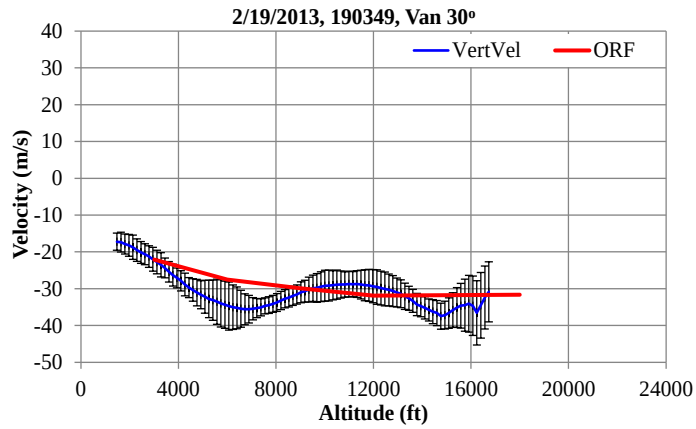
2/19/2013, 190349, Van 30°
Velocity (m/s)
Altitude (ft)
VertVel
ORF

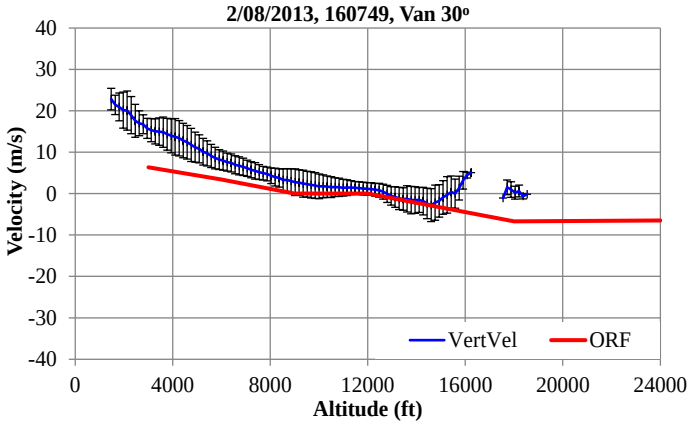
2/08/2013, 160749, Van 30°
Velocity (m/s)
Altitude (ft)
VertVel
ORF

Appendix D

Graphical comparison of wind direction and speed (quantitative analysis results) from ground testing.

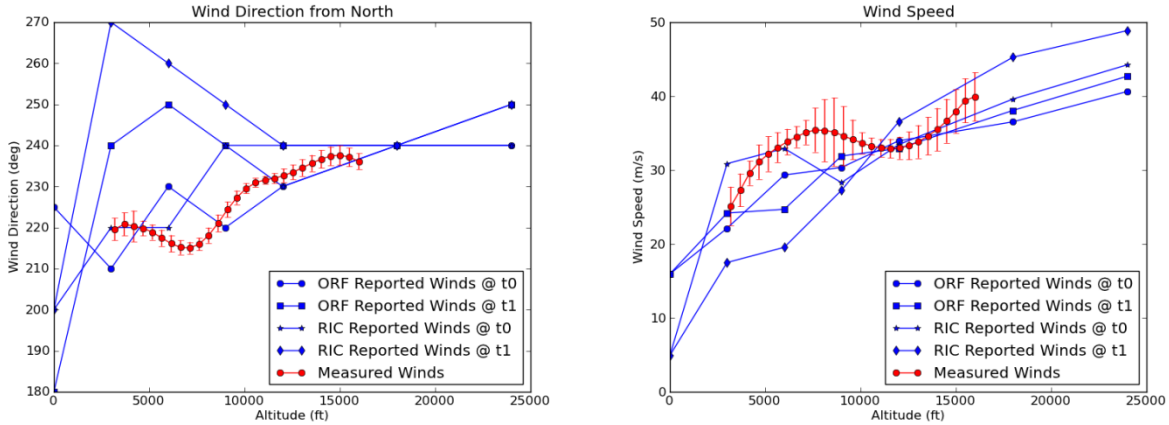

Figure 39: Quantitative Wind Comparison, 2/19/2013, 185548, Van 30^0

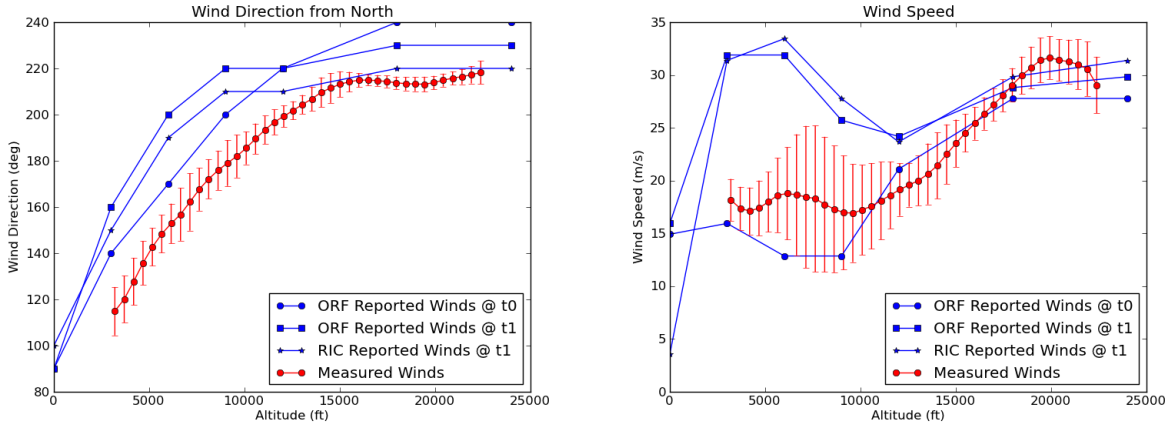

Figure 40: Quantitative Wind Comparison, 2/26/2013, 185057, Van 0^0

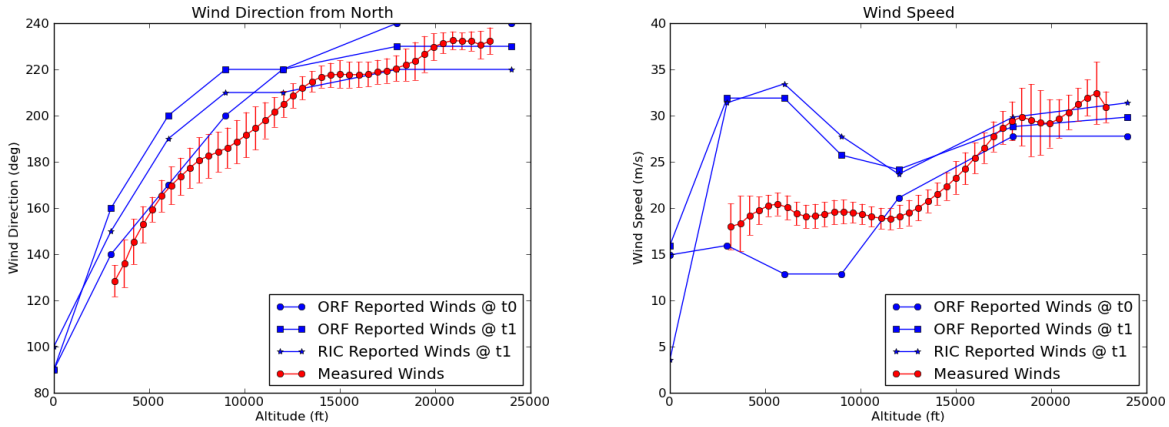

Figure 41: Quantitative Wind Comparison, 2/26/2013, 192836, Van 90^0

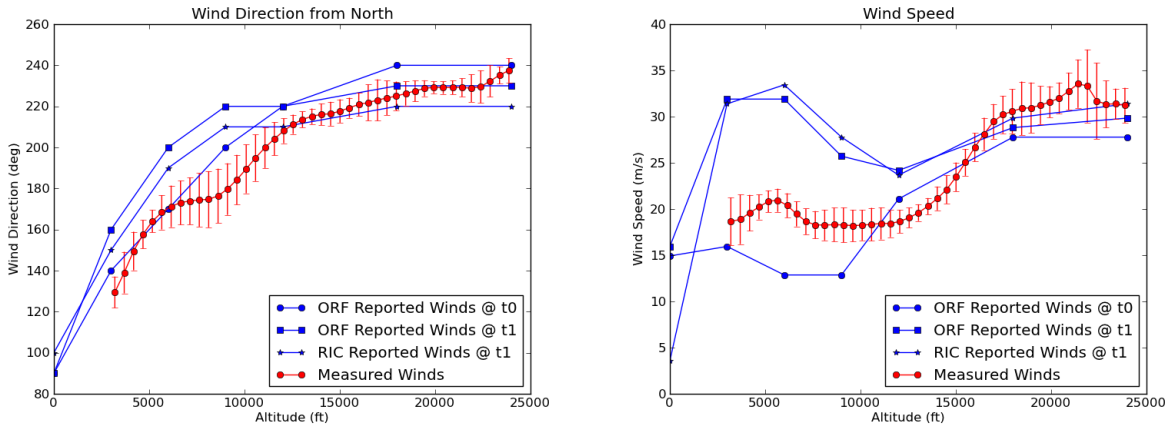

Figure 42: Quantitative Wind Comparison, 2/26/2013, 194045, Van 90^0

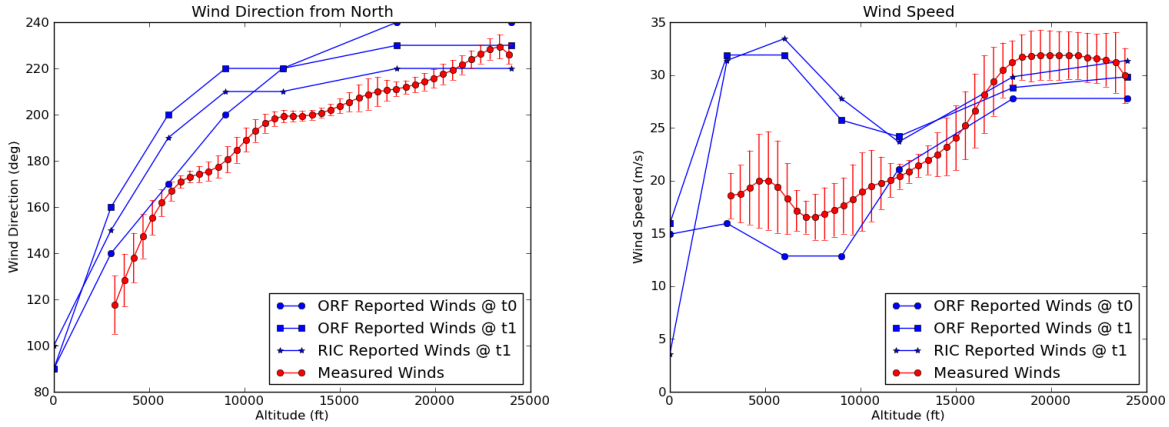

Figure 43: Quantitative Wind Comparison, 2/26/2013, 195327, Van 180^0

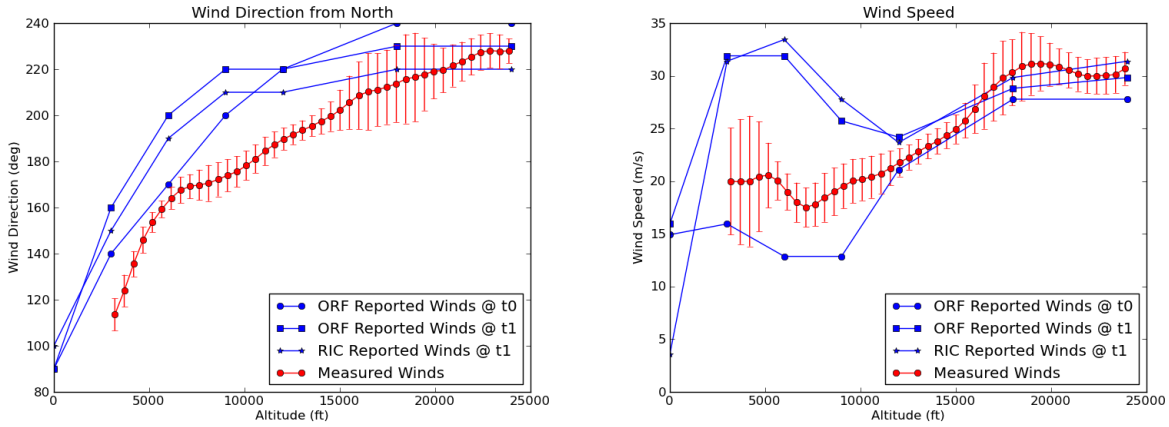

Figure 44: Quantitative Wind Comparison, 2/26/2013, 200258, Van 130^0

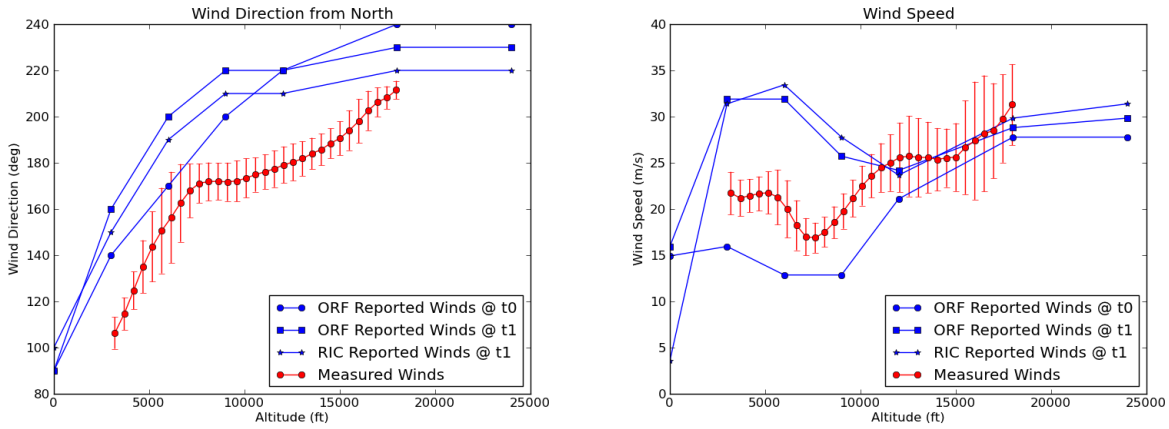

Figure 45: Quantitative Wind Comparison, 2/26/2013, 202611, Van 225^{0}

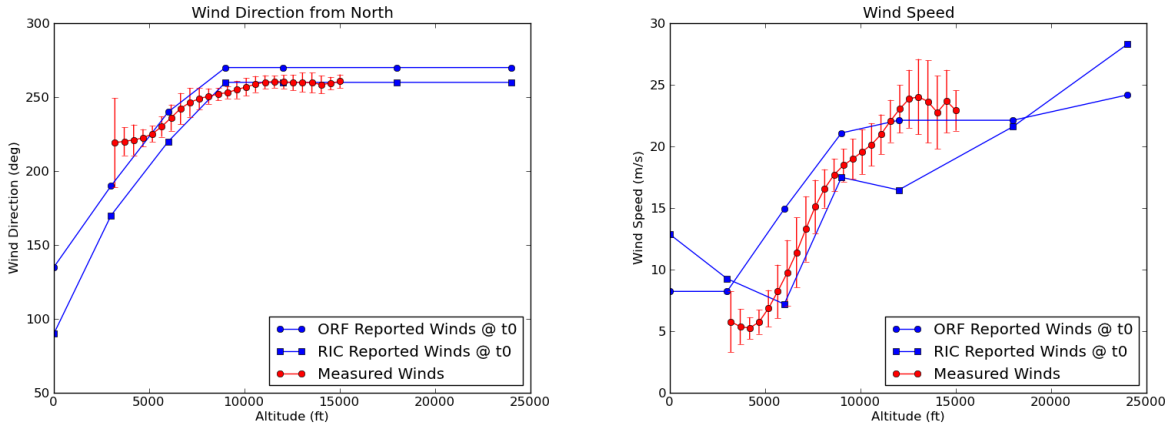

Figure 46: Quantitative Wind Comparison, 3/5/2013, 213913, Van 30^{0}

REPORT DOCUMENTATION PAGE

Form Approved
OMB No. 0704-0188

1. REPORT DATE *(DD-MM-YYYY)*
1-08-2020

2. REPORT TYPE
Technical Memorandum

3. DATES COVERED *(From - To)*

4. TITLE AND SUBTITLE

Process for Detecting Strong Convection Using an Airborne, Doppler, Weather Radar

5a. CONTRACT NUMBER

5b. GRANT NUMBER

5c. PROGRAM ELEMENT NUMBER

6. AUTHOR(S)

Harrah, Steven D.; Hunt, Patricia J.; Strickland, Justin Kyle

5d. PROJECT NUMBER

5e. TASK NUMBER

5f. WORK UNIT NUMBER
80LARC17C0003

7. PERFORMING ORGANIZATION NAME(S) AND ADDRESS(ES)

NASA Langley Research Center
Hampton, VA 23681-2199

8. PERFORMING ORGANIZATION REPORT NUMBER

9. SPONSORING/MONITORING AGENCY NAME(S) AND ADDRESS(ES)

National Aeronautics and Space Administration
Washington, DC 20546-0001

10. SPONSOR/MONITOR'S ACRONYM(S)
NASA

11. SPONSOR/MONITOR'S REPORT NUMBER(S)
NASA-TM-2020-5005042

12. DISTRIBUTION/AVAILABILITY STATEMENT

Unclassified
Subject Category :
Availability: NASA STI Program (757)
864-9658

13. SUPPLEMENTARY NOTES

14. ABSTRACT

This document presents a methodology for producing a measure of the convective wind field ahead of an aircraft using a modern, airborne, Doppler, weather radar. The processes and hardware requirements are consistent with the capabilities found in modern commercial weather radars commonly in use on commercial transport aircraft. The fundamental process is developed as well as results from ground and flight testing are described. This application appears sufficiently mature to allow its use in future NASA flight campaigns that will search for convective cells. If this application continues to perform successfully, it will be recommended to avionics manufacturing colleagues for inclusion into future commercial, airborne, Doppler, weather radars to aide pilots with flight operations and further enhance aviation safety.

15. SUBJECT TERMS

16. SECURITY CLASSIFICATION OF:			**17. LIMITATION OF ABSTRACT**	**18. NUMBER OF PAGES**	**19a. NAME OF RESPONSIBLE PERSON**
a. REPORT	**b. ABSTRACT**	**c. THIS PAGE**			STI Help Desk (email: help@sti.nasa.gov)
U	U	U	UU	44	**19b. TELEPHONE NUMBER** *(Include area code)* (757) 864-9658